國立臺灣大學工學院土木工程學系

碩士論文

Department of Civil Engineering

College of Engineering

National Taiwan University

Master Thesis

基於土地利用與道路影像轉移學習之時空汙染濃度估計

Estimating Spatiotemporal Variations in Pollutant Concentration: Onboard Camera Image Transfer learning and Land Use Regression

費聿暄

Yu-Hsuan Fei

指導教授: 陳柏華 博士

Advisor: Albert Y. Chen Ph.D.

中華民國 111 年 8 月

August, 2022

doi:10.6342/NTU202202826

國立臺灣大學碩士學位論文
口試委員會審定書

National Taiwan University Master Thesis Oral Examination Committee Approval

基於土地利用與道路影像轉移學習之汙染時空濃度估計
Estimating Spatiotemporal Variations in Pollutant Concentration: Onboard Camera Image Transfer learning and Land Use Regression

本論文係費聿暄(R09521515)在國立臺灣大學土木工程學系交通工程組完成之碩士學位論文，於民國 111 年 8 月 09 日承下列考試委員審查通過及口試及格，特此證明。

Yu-Hsuan Fei (R09521515) completed this master thesis at the Department of Civil Engineering Transportation Engineering on August 09, 2022 and passed the oral examination reviewed by the following examination committee members.

口試委員 Oral examination committee members：

陳柏華 （指導教授 Advisor）

蕭大智

張瀞之

系主任 葛宇甯

Acknowledgements

感謝指導教授陳柏華老師，環工所蕭大智老師，交通組的學長姐，環工所的學長姐給予的幫助。碩士的兩年過得非常充實，而且也同時非常自由，陳柏華老師對於我的信任讓我能在這兩年自由的學習跟選擇自己想要的路。教授們與學長姐都給了我很多的指引跟新的觀念，確實的打開了未來的方向，眞的非常感謝。

再來感謝的是我的家人朋友，家人給予我經濟上的支持，讓我安然無恙的讀完碩士，朋友與室友一起分享快樂與壓力，讓我的碩士生活能夠順利，非常感謝。

doi:10.6342/NTU202202826

摘要

空氣污染暴露對人體健康有害。固定測站監測提供了高品質的空氣污染的測量結果，但在估計旅行者在道路上污染暴露的空間變異性時受到限制。此外，它可能導致街道層級的空間變化表徵不佳。因此，移動監測已被廣泛用於收集及時的時空空氣污染測量值。

土地利用回歸 (LUR) 是預測空氣污染物濃度的典型模型。LUR 模型通常利用來自固定監測站點的固定測量值。另一方面，許多研究開始使用移動監測。影像數據和 LUR 可以組成包含固定和移動測量的混合模型。圖像分割技術常用於街景圖像數據處理。然而，大多數深度學習方法都需要標記良好的數據來進行模型訓練。此外，處理數據需要大量的人工工作。

本研究提出了一種用於未標記的車載攝影機影像的遷移學習方法和一種利用 deeplabV2 模型進行圖像分割的圖像特徵提取方法。我們沿著台中台灣大道進行了移動監測，以開發一個混合模型來預測二氧化碳（CO_2）、氮氧化物（NOx）、黑碳（BC）和粒子數（PN）濃度。我們模型的 5 折交叉驗證 R^2 分別爲 CO_2、NOx、BC 和 PN 的 0.79、0.88、0.61 和 0.63。當標記良好的數據難以獲取時，這種遷移學習方法可能會有所幫助。此外，這項工作使混合模型能夠適應不同的車載攝像頭場景，並可用於估計道路污染暴露。

關鍵字：轉移學習、土地利用、影像分割、空氣汙染、汙染濃度

doi:10.6342/NTU202202826

Abstract

Air pollution exposure is harmful to human health. Stationary monitoring of air pollution provides high-quality measurements while limited when estimating spatial variability of on-road exposure of travelers. In addition, it may lead to poor characterization of spatial variation at the street level. Therefore, mobile monitoring has been widely adopted for collecting real-time air pollution measurements.

The Land Use Regression (LUR) is a typical model for predicting air pollutant concentrations. LUR models usually utilize stationary measurements from fixed monitoring sites. On the other hand, numerous studies took measures from mobile monitoring sources. Image data and the LUR can form a hybrid model with stationary and mobile measurements. The image segmentation technique is often used for street view image data processing. However, most deep learning methods require well-labeled data for model training. In addition, it needs a lot of human work to process data.

This study presents a transfer learning approach for unlabeled onboard camera images and an image feature extraction approach utilizing image segmentation with the deeplabV2 model. We conducted mobile monitoring along Taiwan Avenue, Taichung, to develop a hybrid model to predict carbon dioxide (CO_2), nitrogen oxides (NOx), black carbon (BC), and particle number (PN) concentration. The 5-fold cross-validation R^2 for our model was 0.79, 0.88, 0.61, and 0.63 for the CO_2, NOx, BC, and PN, respectively. This transfer learning method may be helpful when well-labeled data is difficult to acquire. Furthermore, this work enabled the hybrid model to adapt to different onboard camera

doi:10.6342/NTU202202826

scenarios and can be applied to estimate the on-road pollution exposure.

Keywords: transfer learning, land use, image segmentation, air pollution, pollutant concentrations

doi:10.6342/NTU202202826

Contents

doi:10.6342/NTU202202826

doi:10.6342/NTU202202826

List of Figures

doi:10.6342/NTU202202826

doi:10.6342/NTU202202826

List of Tables

doi:10.6342/NTU202202826

Chapter 1 INTRODUCTION

Over the past decade, air pollution has been a severe environmental problem. Greenhouse emissions affect climate change [1, 2]. In the transportation field, the average annual greenhouse gas (GHG) emissions growth remained roughly constant at about 2% per year [3]. In comparison to the transport sector, the average annual GHG emissions growth slowed in energy supply and industry. Air pollution exposure is also harmful to human health [4–8]. Especially for commuters, air pollution is generated by them and affects them. Motorcyclists are more easily and have higher exposure to air pollution than other commuters [9]. These severely impact human health in those countries with many motorcyclists, such as Vietnam and Taiwan [10, 11]. However, it is hard to evaluate the risk that commuters expose to. Pollutant concentrations have spatiotemporal variation and can change rapidly in and short time and distance [12–14].

1.1 Stationary and mobile monitoring

Traditional stationary monitoring is a common method of measuring air pollution. In most regions around the globe, ambient air pollution and quality are monitored at stationary stations. The networks of stationary stations provide high-quality measurements of air pollution while limited when estimating spatial variability of on-road exposure of travelers. It may lead to poor characterization of spatial variation at the street level [15–18]. Mobile monitoring effectively estimates spatial patterns of pollutant concentrations, but it needs repeated measurements to map the general air pollution patterns [19, 20]. Es-

doi:10.6342/NTU202202826

timating air pollutant concentrations is a trade-off between accuracy and efficiency. Both types of monitoring have their pros and cons.

1.2 Emerging technologies

Land use regression (LUR) is a typical model for predicting air pollutant concentrations [21–25]. LUR models usually utilize stationary measurements from fixed monitoring sites to estimate pollutant concentrations [21]. On the other hand, numerous studies took measures from mobile monitoring sources. While emerging mobile monitoring and the LUR model, plenty of works introduce street view imagery to provide more detailed spatial information and match the spatial scale of the collected measurements [26–30]. Some studies have collected their street view imagery and measurements. Hankey et al. [31] used bicycle-based, mobile measurements. Liang et al. [32] used remote sensing images. Liu et al. [33, 34] used portable pollution monitoring devices. They used image segmentation to extract features from GSV imagery. Others also have used Google Street View (GSV) imagery [29, 35–38]. GSV dataset is a good dataset for estimating pollutant concentrations. The limitation of GSV is it has temporal mismatch and a lack of temporal resolution. GSV images are shoot at a different time from the pollutant concentrations measurements and have low time resolution. Except for the GSV dataset, collecting and processing street view image data is time-consuming. Therefore, these methods have limitations due to the heavy work of collecting and processing image data. This means that applying the model to a different dataset or country is complex.

doi:10.6342/NTU202202826

1.3 Objective

In this study, we used a mobile monitoring vehicle to monitor the exposure of four types of pollution to the commuter along Taiwan Boulevard, Taichung, and collect street view images with an onboard camera at the same time to predict four types of air pollutants, carbon dioxide (CO_2), nitrogen oxides (NOx), black carbon (BC) and particle number (PN). We present a transfer learning approach for unlabeled onboard camera images and an image feature extraction approach utilizing image segmentation with the deeplabV2 model [39, 40]. We develop a hybrid regression model with predictor variables derived from onboard camera imagery and land use. The primary goals of this study were :

1. Testing the workflow of transfer learning to increase universality of models
2. Providing spatiotemporal variability of CO_2, NOx, BC, and PN concentrations
3. Improving model robustness and interpretability by testing different parameters

This transfer learning method may be helpful when well-labeled data is challenging to acquire. This work enabled the hybrid model to adapt to different onboard camera scenarios and can be applied to estimate the on-road pollution exposure.

doi:10.6342/NTU202202826

Chapter 2 LITERATURE REVIEW

We are going to talk about the previous works. This chapter has four parts. First, we figure out the pros and cons of the monitoring method. Next, we find different land use regression models and machine learning methods. After that, we took a look at the deep learning methods and street view imagery. The final part is the research gap.

2.1 Monitoring

The previous chapter mentions that air pollution concentrations are typically measured at a stationary monitoring network. Stationary monitoring may lead to poor characterization of spatial variation at the street level. Apte et al. [12] indicated that air pollution changes sharply over distances shorter than one kilometer. The fixed-site monitoring has a less spatial resolution. They introduced a measurement approach that equipped a pollution measurement platform on Google Street View vehicles. Their scalable approach has shown the potential of mobile monitoring. Besides, Chen et al. [19] suggested that mobile monitoring needs repeated measurements to map the general air pollution patterns. It is time-consuming for repeated work and will take much time and effort to a larger or more complicated region.

2.2 Land use regression

LUR models have been widely used for modeling spatial variation in air pollution concentrations. Eeftens et al. [21] measured the concentrations of $PM_{2.5}$, $PM_{2.5}$ ab-

doi:10.6342/NTU202202826

sorbance, PM_{10}, and PM_{coarse} in 20 European study areas at 20 sites per area. Their ESCAPE project used land use predictor variables along with traffic intensity and population in the regression model to evaluate spatial variation. They indicate that careful selection of monitoring sites was essential for developing stable LUR models. Their research used stationary monitoring networks to measure air pollution concentrations. The LUR model is usually used on a large spatial scale. Schmitz et al. [22] introduce the potential of spatial aggregations. They used the land use regression model from the ESCAPE project and calculated it into a dataset on the $5 \times 5m$ grid covering the entire Netherlands. They combined the air pollution maps with personal mobility and activity patterns in high-resolution datasets. Their dataset can spatially aggregate to different scales and estimate individual exposure.

In addition to the regression model, Wu et al. [25] developed land use machine learning models to estimate hourly emissions of vehicular pollutants based on traffic monitoring. Their measurement method is similar to stationary monitoring, while they introduced machine learning methods to improve the performance of the land use model. Their research demonstrated the power of land-use random forest (LURF) to estimate high-resolution emissions and provided a platform to estimate near-real-time vehicle emissions. Rundle et al. [29] used GSV data to audit the seven neighborhood environment constructions.

2.3 Street view imagery

Geographic Information Systems (GIS) is the major recourse of Land use variables. The GIS-derived predictor variables are available at larger geographic scales, while the mobile monitoring is conducted on a smaller spatial scale. Therefore, plenty of works

doi:10.6342/NTU202202826

introduced the GSV imagery. Li et al. [35] used GSV to assess street-level greenery. They modified Green View Index (GVI) fomula and combined GVI with GSV. Stubbings et al. [36] used a deep learning model to detect the areas of vegetation. They combined the information from several images of the deep learning results to form an indicator of greenery. They compared their model with an image segmentation method based on a pre-labeled dataset. Seiferling et al. [37] introduced an algorithm estimating the tree cover in GSV images. They measured the amount of tree cover in city streetscapes by modeling the relationship between neighboring images and city streets. Ganji et al. [41] developed algorithms to extract built environment features from GSV images. They used these features to train a Bayesian regularized artificial neural network (BRANN) model to predict near-road air quality. They also compare with other neural networks and the land-use regression model. Qi et al. [38] used an image segmentation model to extract features from GSV imagery. They developed a LUR model based on mobile monitoring data and images to predict air pollution concentration. However, Rzotkiewicz et al. [42] indicated advantages of using GSV imagery included lower cost, usability, and time saved. Disadvantages were spatial and temporal availability, largely in developing regions of the world.

Instead of using GSV data, Liu et al. [33, 34, 43] used their imagery captured by a mobile platform along with BC measurements. They introduced a model based on street view images and meteorological data to discover the driving factors of the spatial variability at a higher spatial resolution.

2.4 Research gap

From the literature review, the research gap is identified to be the following.

doi:10.6342/NTU202202826

1. Limitation of GSV, high cost of collecting imagery, and the inflexibility of machine learning

   The combination of land use and mobile monitoring has been proved to be a promising method to predict air pollution concentrations. As for the imagery data, it has a temporal mismatch and a lack of temporal resolution. GSV images are shot at a different time from the pollutant concentrations measurements and have low resolution. It is also restricted by the usability and accessibility of Google Street View vehicles. Collecting and processing street view image data is time-consuming except for the GSV dataset. Besides, the machine learning model fits the training dataset, and using the machine learning method requires lots of effort to prepare and process images. It costs much to prepare another dataset for training.

2. Lack of greenhouse gas

   Most research focused on BC, PN, and NOx concentrations. However, greenhouse gases (GHGs) are also a significant transportation emission [44]. Moreover, climate change has both directly and indirectly affected human health in China, including extreme weather events, air, and water quality changes, and the ecology of infectious diseases [2]. Therefore, we believe that CO_2 is necessary to be estimated in the transportation field.

3. Limitation of linear regression

   Linear regression is a promising method that can explain data variability. However, linear regression may be hard to capture complex interactions and cannot estimate non-linear relationships between pollutant concentrations, land use variables, and image variables. Many studies showed the potential of the traditional land use regression model [45–49]. We considered the combination of land use and street view

doi:10.6342/NTU202202826

imagery more complicated than the traditional land use regression. Therefore, we want to apply the random forest model and fine-tune the hyperparameters and parameters to find the best performance.

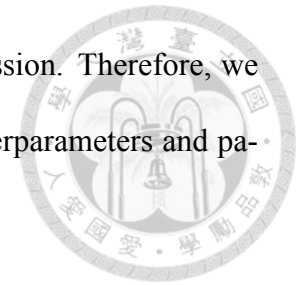

doi:10.6342/NTU202202826

Chapter 3 METHODOLOGY

We are going to introduce our methodology in this chapter. Figure 3.1 is the total flow chart of our work. We first use the transfer learning method to transfer the open-source dataset, then train the segmentation model with transferred images. After that, we extract the image predictor variables with the trained segmentation model and land use predictor variables from the land use image. Finally, we use these predictor variables to train the random forest regression model.

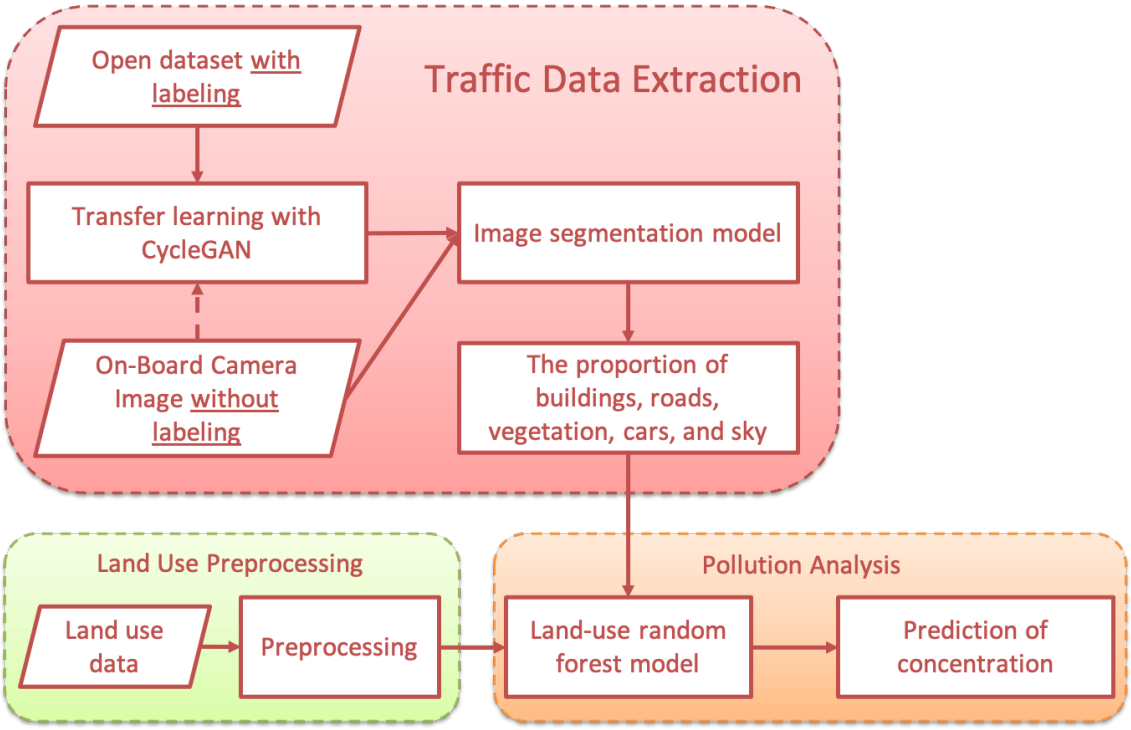

Figure 3.1: Total workflow

3.1 Transfer learning with the CycleGAN model

Most previous works need a well-labeled dataset to extract features from imagery. However, preparing a well-labeled dataset is time-consuming. We try to reduce the cost

doi:10.6342/NTU202202826

of applying the model to another dataset with transfer learning. Transfer learning captures essential information learned from the procedure of solving one problem (source domain) and using it for a different but related problem (target domain). We prepare an already well-labeled and reliable open-source dataset belonging to the source domain (X). The mobile measurement we collect along Taiwan Boulevard, Taichung, belongs to the target domain (Y). We hope the deep learning model could be trained by the open-source dataset after the domain transfer and can process data collected along Taiwan Boulevard.

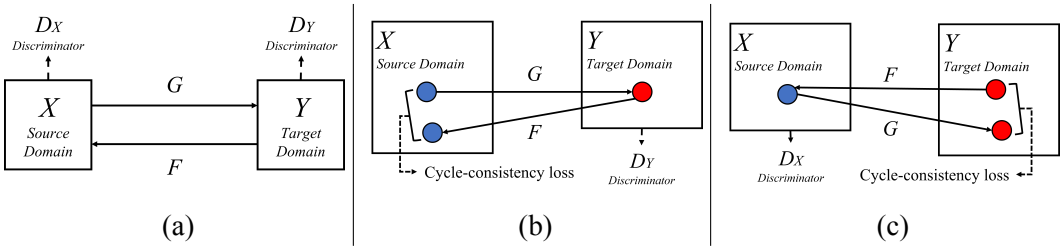

Figure 3.2: (a) CycleGAN contain two mapping functions G and F, and discriminators D_Y and D_X. (b) Forward cycle-consistency loss. (c) Backward cycle-consistency loss

CycleGAN (Figure 3.2) is selected as the transfer learning model for the image-to-image translation [39]. It contained two generative adversarial networks for mapping: mapping the X to the Y and mapping the Y to the X (F). There are two associated adversarial discriminators D_Y and D_X. D_Y encourages G to translate X into Y, and vice versa for D_X and F. Those mappings should be cycle-consistent with cycle consistency loss and guarantee that both mappings won't lose any critical feature. It does not need paired training data and has obtained promising results in problems such as collection style transfer, season transfer, and photo enhancement.

We use CycleGAN as the transfer learning model with the open-source dataset Cityscapes as the source image data and our onboard camera image as the target image (Figure 3.3). We used the source and target images to train the CycleGAN model and then stylized the source image's domain to the target image's domain.

doi:10.6342/NTU202202826

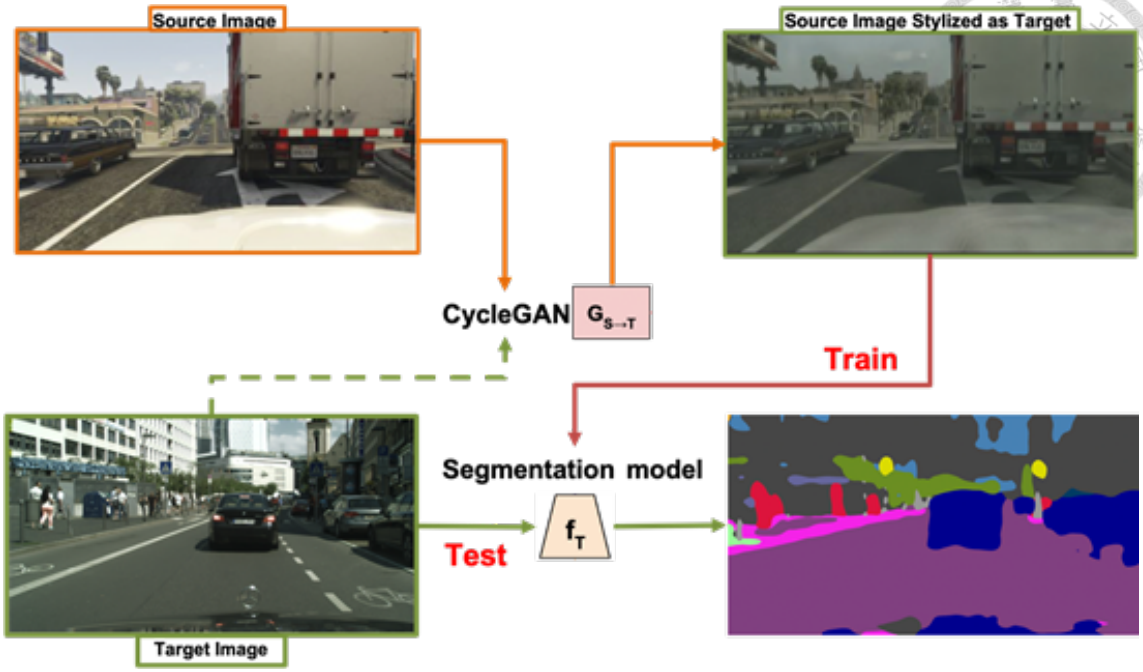

Figure 3.3: Transfer learning workflow

3.2 Predictor variables extractor

After transfer learning, we extract the feature as predictor variables from imagery with image segmentation (Figure 3.3). We use DeeplabV2 [40]. DeeplabV2 is a semantic segmentation algorithm that builds on Deeplab with an atrous spatial pyramid pooling (ASPP) scheme (Figure 3.4). Atrous convolution is a filter 'with holes'. We can compute responses at all positions of images if we convolve the full resolution image with atrous convolution and do not lose information during the downsampling and upsampling. ASPP consists of multiple parallel atrous convolution layers with different sampling rates. ASPP extracted features for each sampling rate. These features are then processed in separate branches and fused to generate the final result. ASPP help to capture objects and context at different scales. DeeplabV2 has a relatively simple structure and fast training speed. This model classifies the pixel into 19 classes. We use the count of each class as the predictor variables for another regression model to predict pollutant concentration.

doi:10.6342/NTU202202826

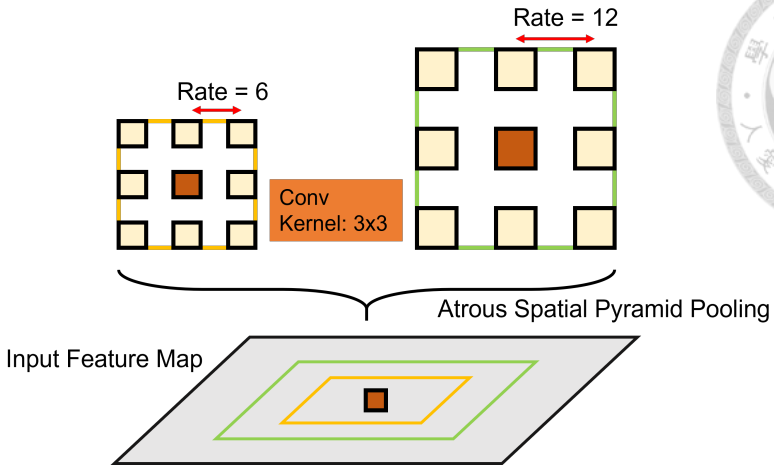

Figure 3.4: ASPP of Deeplab

As for land-use predictor variables, we calculate the 133 classes (B.10) of land use within a round buffer area with different buffer radius sizes (Figure 3.5 and B.11). (i.e., seven buffer sizes from 100 to 700 m). The land use data comes from Nation Land Surveying and Mapping Center in imagery form. We count pixels of every type of land use at every measurement point as the land use variables.

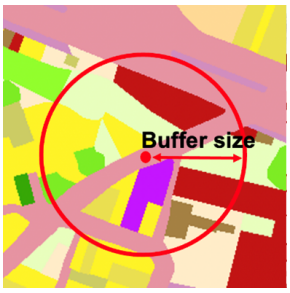

Figure 3.5: Land use imagery and buffer size

3.3 Random Forest Regression model

The random forest regression model [50, 51] has been shown to perform well in predicting pollutant concentration [34]. We combine image segmentation results and land use data as variables to develop a random forest regression model. The variables' classes and numbers are shown in Table 3.1. With the random forest regression model, we can predict pollutant concentration. We adjust the hyperparameters to find better performance.

doi:10.6342/NTU202202826

We defined the HYBRID model as the regression model using all variables, the LU model using land use variables, and the SEG model using image segmentation variables.

The accuracy evaluation reflects the model's quality. We use 5-fold cross-validation to estimate the model performance. Cross-validation can reduce the random error from the random sample procedure. Both the R-square (R^2) and the root mean square error (RMSE) were used as metrics to evaluate the model performance. The mean R^2 of 5 subsets was reported as the 5-fold cross-validation R^2.

Table 3.1: The predictor variables for HYBRID, LU and SEG model

Model		Factors	Example Variables	Total Number of Factors	Data source
HYBRID	LU	Land use	Agriculture (01), Forest (02), Transportation (03), Water Resources (04), Architecture (05), Public (06), Recreation (07), Mineral and Salt (08), Others (09)	133	Nation Land Surveying and Mapping Center
		Meteorological variables	Station pressure, Temperature, Relative humidity, Wind speed, Wind direction, Precipitation	16	Central Weather Bureau, Fixed monitoring station
	SEG	Street view image	Flat, Human, Vehicle, Construction, Object, Nature, Sky, Void, Speed	20	Camera

doi:10.6342/NTU202202826

Chapter 4 RESULTS

In this chapter, we demonstrate our results of the regression model. The indicator is R^2. There will be three parts. The first part is related to our data.

4.1 Mobile monitoring data

The mobile monitoring data was collected in Taichung, Taiwan.(Figure 4.1 and 4.2) It is the second-largest city in Taiwan. The mean annual temperature and rainfall are 23.7°C and 1762.8 mm (1991-2020). We conducted vehicle mobile monitoring to measure daytime street-level pollutant concentrations along Taiwan Boulevard, Taichung. We deployed LI-7815 from LI-COR, nCLD 88 p from ECO PHYSICS AG, MA350 from AethLabs, and MAGIC 210 from Aerosol Devices Inc. on the same vehicle to measure CO_2, NOx, BC, and PN concentrations at 2 s resolution simultaneously. It was equipped with a GPS to register the measurement location at 1 s resolution and an onboard camera in front of the vehicle to record the street view images with 25 frames per second. Taiwan Boulevard was repeatedly sampled for two hours in the morning and noon for seven days in September 2020.

We use these data from Yeh [52]. In that paper, they also conduct the rolling minimum to estimate background concentrations (BKG). The rolling minimum is a widely used method for estimating BKG from time series. This method sets a window rolling over the data and calculates the minimum values within the window. In this study, we defined the measurements as total concentration (TOTAL). We apply the BKG, estimated in Yeh,[52]

doi:10.6342/NTU202202826

Figure 4.1: Mobile monitoring route

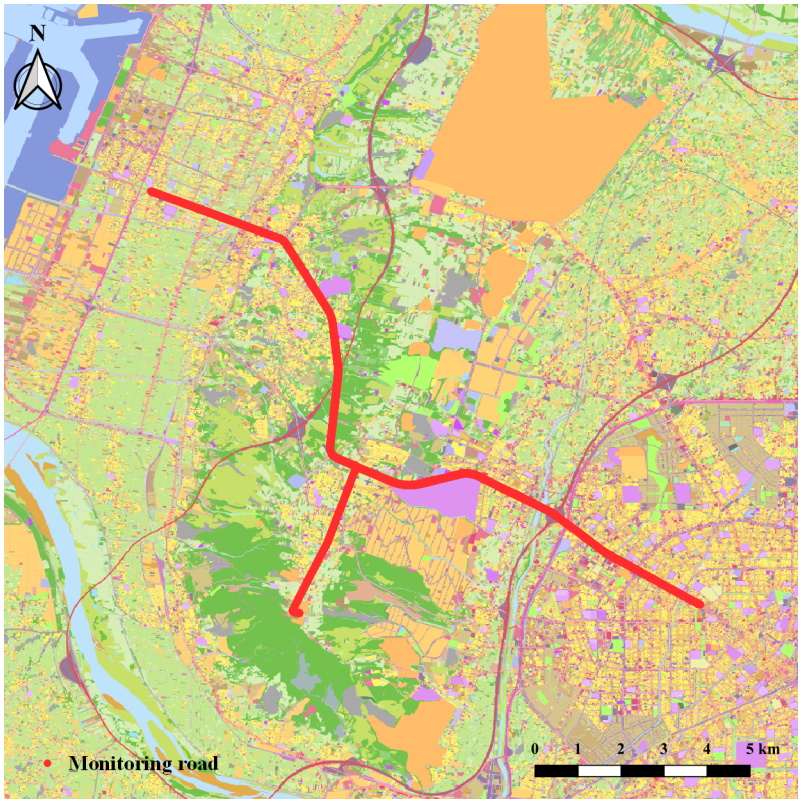

Figure 4.2: Route and land use

doi:10.6342/NTU202202826

and define the difference (DIF) as the Total minus the BKG values. The street view images (320×160 pixels) were upscaled to 2048×1024 pixels. After being processed with transfer learning and semantic segmentation, we divided the image pixel into 19 classes and used each class's counts as predictor variables. For land use variables, we use the pixel counts of each land use class in a round buffer with a specific buffer size, which is 0.54×0.54 m for the one-pixel size of land use data. The predictor variables also include temperature, relative humidity, wind speed, and pressure measured by a Taichung, Taiwan station operated by Central Weather Bureau close to our measure area.

The pollutant concentration data has 12 subsets derived from different days. Depending on that day's scenario, they have different temporal distributions (Figure 4.3). Therefore, the method that split the training and testing set greatly influenced the model performance. Most previous works use the random sampling method to do cross-validation. If we randomly sample the testing set, the performance might be good. However, random sampling doesn't match the actual applications. Random sampling will probably select the data in the middle as testing data, which the model was already training with those ahead and behind. When we want to apply the model, we won't get any information after the testing time. The model performance estimating with random sampling cannot precisely describe how the model will work in real applications. To match the reality, we can randomly select one day as testing set closer to the actual application when applying the model. However, the model's performance might not be good as the random sample method because of the variance between subsets. Therefore, we tested both ways and tried to find solutions. We first experiment with the random sample method, then investigate the possibility of testing one day.

doi:10.6342/NTU202202826

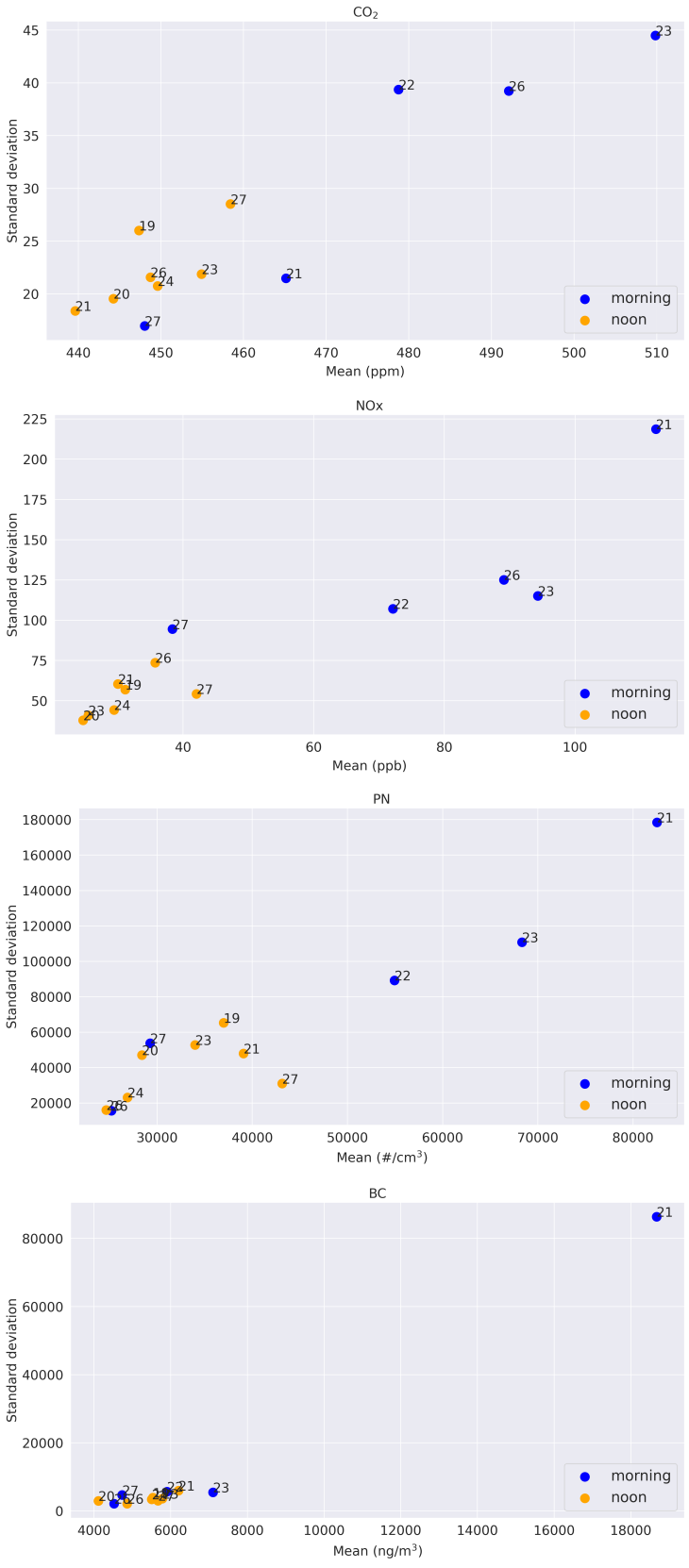

Figure 4.3: Data distribution

doi:10.6342/NTU202202826

4.2 Transfer learning results

As shown in Figure 4.4, the DeeplabV2 model pretrained on the Cityscapes dataset without transfer learning misclassified some classes on our dataset. The road is misclassified to the deep blue class of cars. The model classified objects better with transfer learning. The final R^2 will show in the next section.

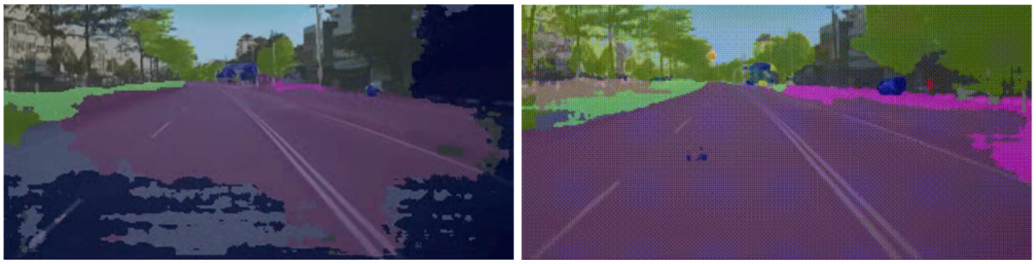

(a) DeeplabV2 without transfer learning (b) DeeplabV2 with transfer learning

Figure 4.4: Transfer learning result

4.3 Random sample method

We randomly split the data into five folds and selected each as testing data and the other four as training data. The final R^2 is the mean of five folds. Overall, we get good model performance for the HYBRID model. As shown in Figure 4.5, Figure 4.6, Figure 4.7 and 4.1, the 5-fold CV R^2 for the buffer size 700 meters HYBRID model predicting Total was 0.79, 0.63, 0.61, and 0.88 for the CO_2, NOx, PN, and BC respectively.

For CO_2, image segmentation variables help the land use variables to estimate the concentrations in the HYBRID model. The segmentation variables provide micro information of traffic and road above the LU model. The HYBRID model of predicting BKG has the best performance of all combinations; the second best is. Several factors can explain this. CO_2 concentration barely changes in a short time interval. BKG leads the concentration change, and the DIF is a stochastic effect from the traffic and other resources.

doi:10.6342/NTU202202826

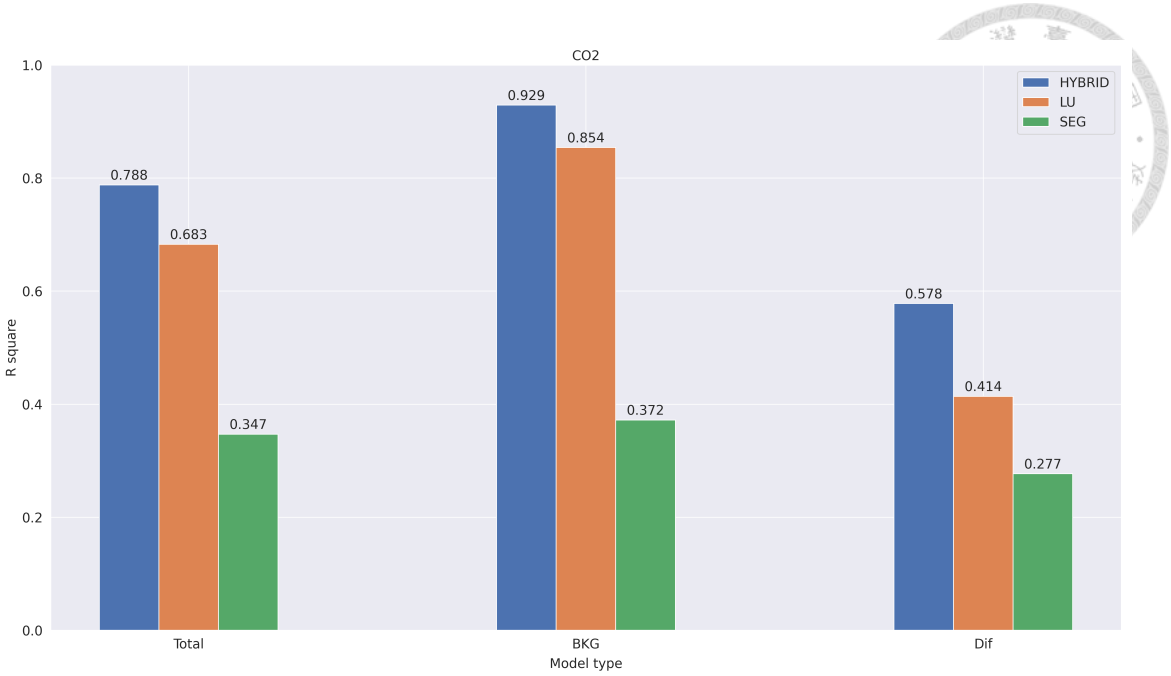

Figure 4.5: HYBRID model 5-fold CV R^2 for the buffer size 700m (1/3)

The close R^2 of the SEG model on Total and BKG also implies that the BKG concentration is important to CO_2. Therefore, the HYBRID model R^2 of Total increases from DIF after combining with BKG. The rolling minimum method can be a factor that causes the best R^2 of BKG. BKG is calculated by the rolling minimum. It should be very smooth and more straightforward to predict than the Total and DIF. Smooth data is easy to predict by the random forest regression model.

NOx and PN have similar patterns of R^2 to CO_2. The data distribution also shows that CO_2, NOx, and PN have identical patterns. The HYBRID model has the best performance among the three models on three kinds of concentration. BKG R^2 of the HYBRID model is higher than Total and DIF. However, BKG's influence on NOx and PN is insignificant compared to CO_2. Unlike CO_2, Total R^2 is very close to the DIF. The total R^2 of the SEG model is also close to the DIF. It means DIF results already can represent the Total. The high R^2 of BKG might come from the stable characteristic of the BKG.

As for BC, the data distribution is different from the others, and the R^2 results are

doi:10.6342/NTU202202826

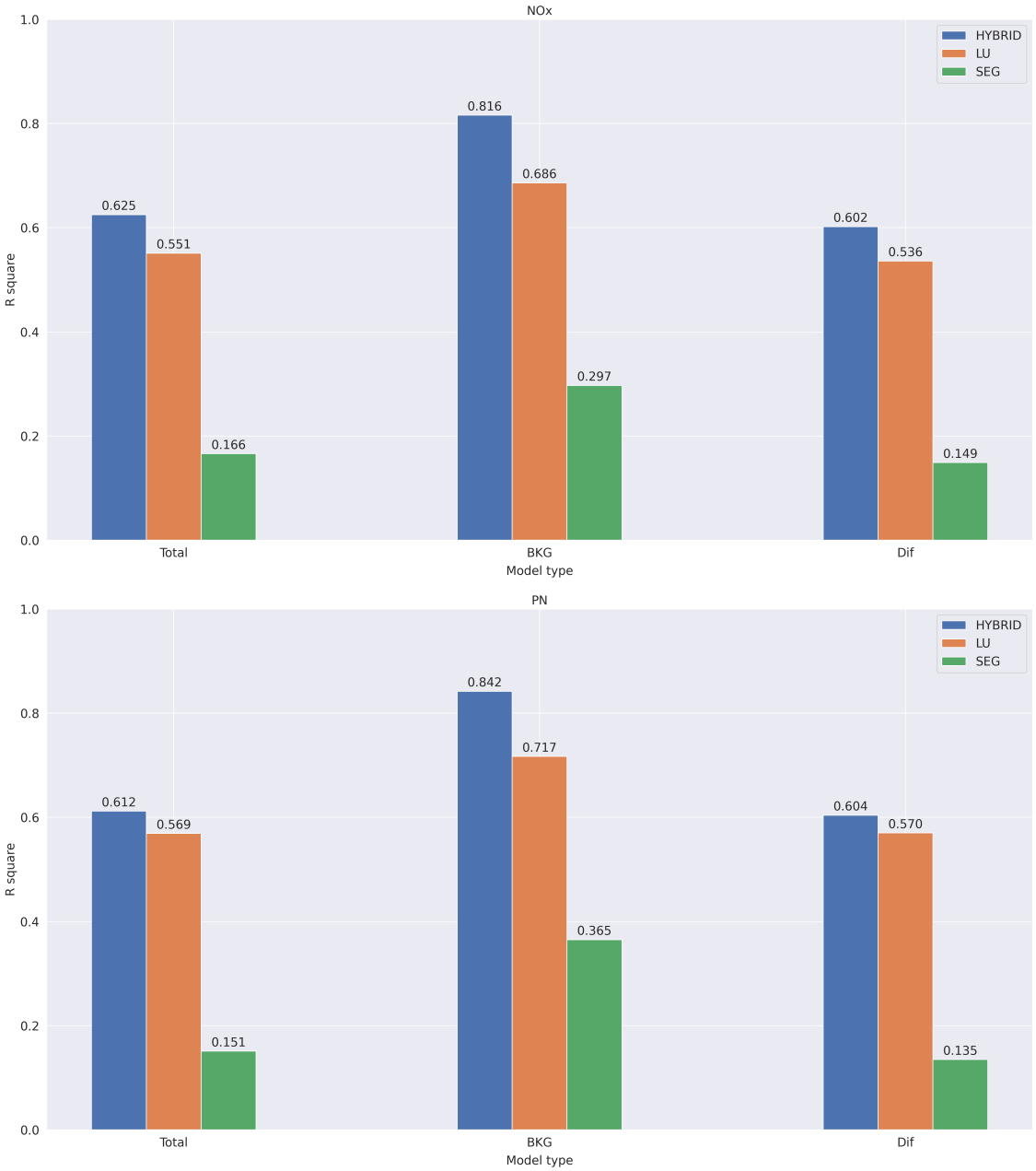

Figure 4.6: HYBRID model 5-fold CV R^2 for the buffer size 700m (2/3)

doi:10.6342/NTU202202826

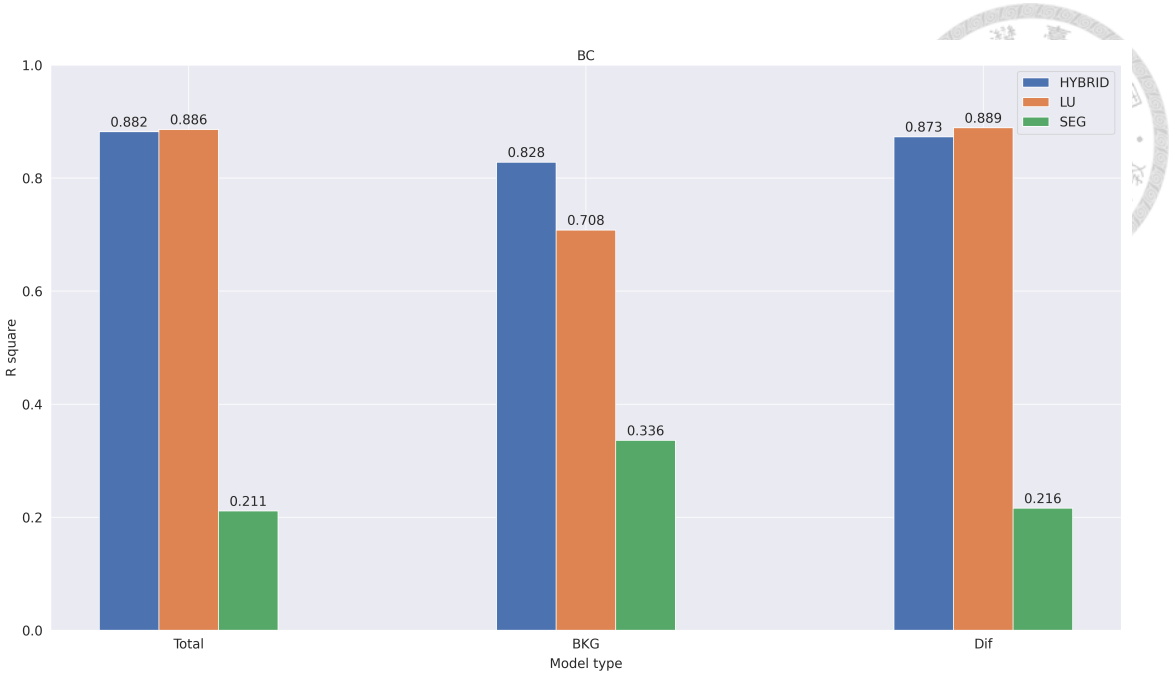

Figure 4.7: HYBRID model 5-fold CV R^2 for the buffer size 700m (3/3)

very different. Total and DIF have similar patterns and performances for model types, which means BC is probably led by the DIF as expected. Most BC concentrations come from DIF. We expected that BC is related to the DIF concentration, and SEG can provide the micro information to help the LU model. However, the relation between DIF and SEG is not significant according to our results. The SEG model even decreases the LU model performance when combined into the HYBRID model. We suppose other factors cannot catch by the imagery data affecting the BC concentrations. The physical effects like the wind have not yet been considered in our regression model. This might cause some prediction errors.

HYBRID and LU model related to the buffer size, so we adjusted it to find a proper one. As shown in Figure 4.8, Figure 4.9 and 4.1, all pollutants have the same kind of patterns. The model performance is good and close for buffer sizes larger than 500 m. The smaller buffer size needs fewer computing resources. We suggest that 500 m is balanced between computing time and performance. The larger buffer size has better perfor-

doi:10.6342/NTU202202826

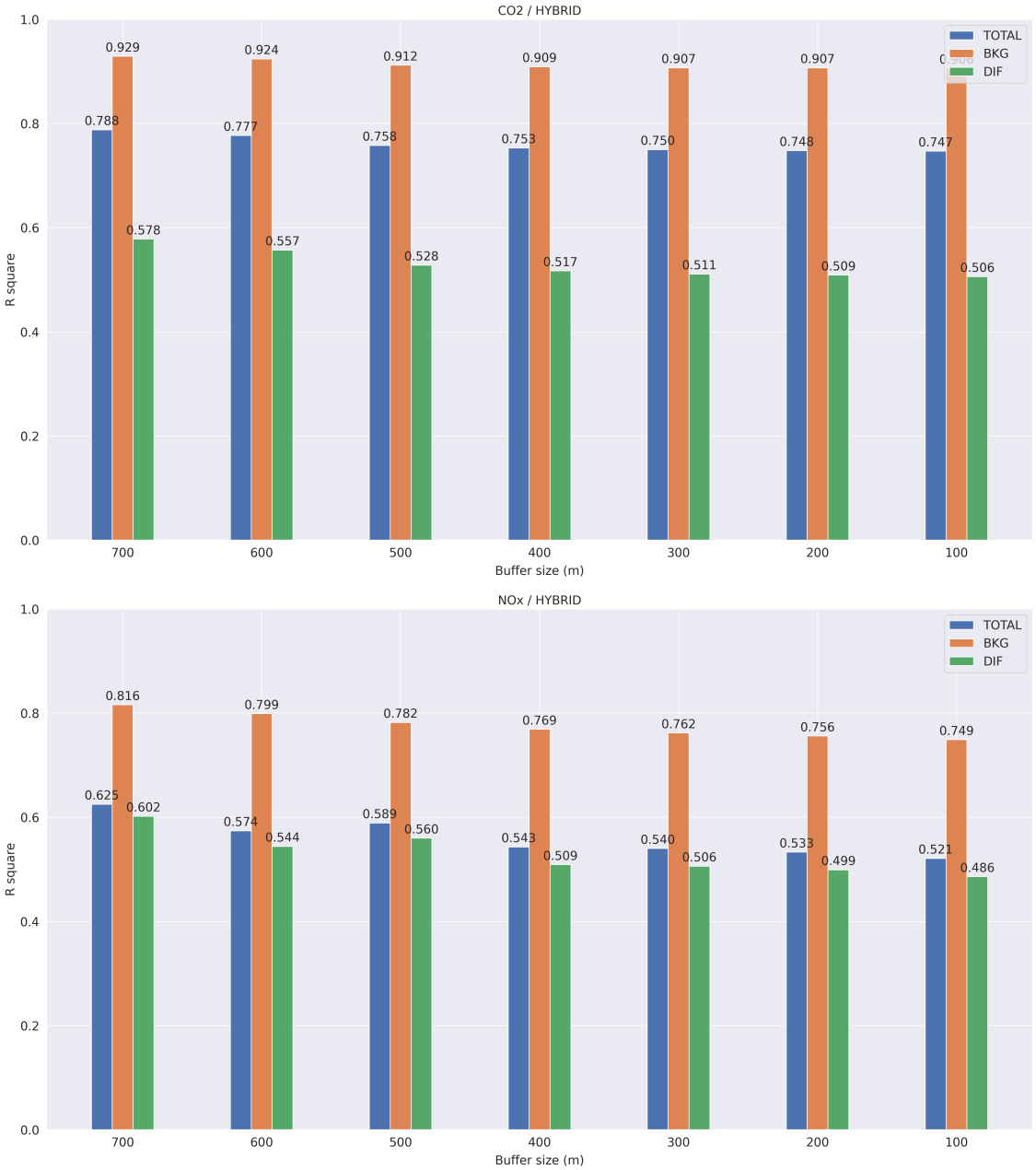

Figure 4.8: Sensitivity analysis of buffer size (1/2)

doi:10.6342/NTU202202826

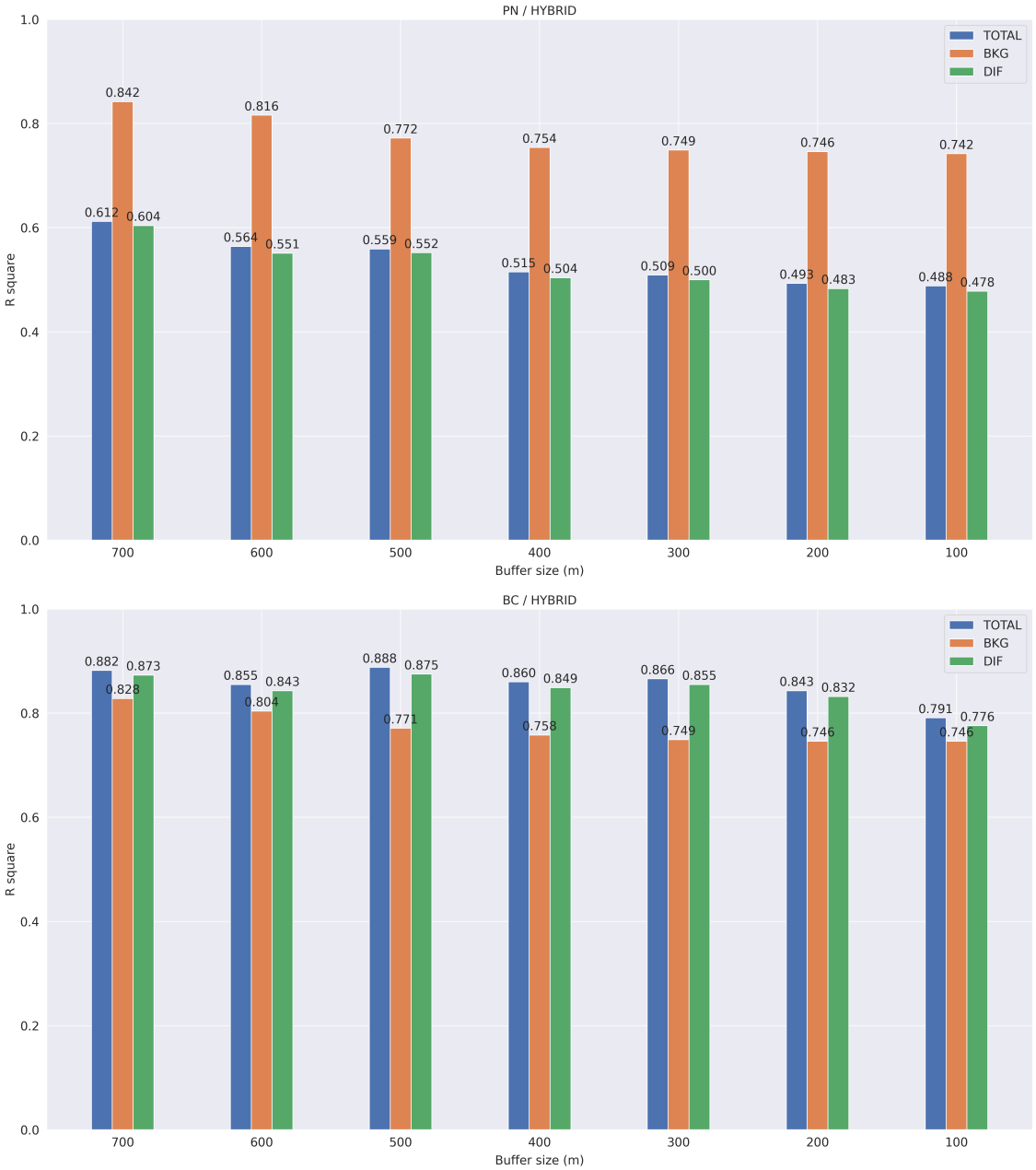

Figure 4.9: Sensitivity analysis of buffer size (2/2)

doi:10.6342/NTU202202826

Table 4.1: R^2 of random sample method with transfer learning

Pollutants	Model types	Concentration types	Buffer size (m)						
			700	600	500	400	300	200	100
CO_2	HYBRID	TOTAL	0.788	0.777	0.758	0.753	0.75	0.748	0.747
		BKG	0.929	0.924	0.912	0.909	0.907	0.907	0.906
		DIF	0.578	0.557	0.528	0.517	0.511	0.509	0.506
	LU	TOTAL	0.683	0.659	0.584	0.574	0.565	0.562	0.552
		BKG	0.854	0.84	0.798	0.791	0.787	0.785	0.783
		DIF	0.414	0.375	0.261	0.243	0.228	0.222	0.205
	SEG	TOTAL	0.347	0.347	0.347	0.347	0.347	0.347	0.347
		BKG	0.372	0.372	0.372	0.372	0.372	0.372	0.372
		DIF	0.277	0.277	0.277	0.276	0.277	0.277	0.277
NOx	HYBRID	TOTAL	0.625	0.574	0.589	0.543	0.54	0.533	0.521
		BKG	0.816	0.799	0.782	0.769	0.762	0.756	0.749
		DIF	0.602	0.544	0.56	0.509	0.506	0.499	0.486
	LU	TOTAL	0.551	0.474	0.431	0.369	0.361	0.352	0.311
		BKG	0.686	0.656	0.604	0.581	0.569	0.558	0.546
		DIF	0.536	0.458	0.41	0.344	0.337	0.327	0.285
	SEG	TOTAL	0.166	0.167	0.167	0.167	0.167	0.168	0.168
		BKG	0.297	0.297	0.298	0.297	0.298	0.297	0.297
		DIF	0.149	0.149	0.149	0.15	0.149	0.149	0.149
PN	HYBRID	TOTAL	0.612	0.564	0.559	0.515	0.509	0.493	0.488
		BKG	0.842	0.816	0.772	0.754	0.749	0.746	0.742
		DIF	0.604	0.551	0.552	0.504	0.5	0.483	0.478
	LU	TOTAL	0.569	0.486	0.413	0.36	0.346	0.328	0.315
		BKG	0.717	0.665	0.532	0.503	0.483	0.467	0.456
		DIF	0.57	0.477	0.413	0.358	0.345	0.328	0.315
	SEG	TOTAL	0.151	0.151	0.152	0.152	0.152	0.152	0.152
		BKG	0.365	0.365	0.365	0.364	0.364	0.364	0.365
		DIF	0.135	0.134	0.134	0.134	0.135	0.135	0.135
BC	HYBRID	TOTAL	0.882	0.855	0.888	0.86	0.866	0.843	0.791
		BKG	0.828	0.804	0.771	0.758	0.749	0.746	0.746
		DIF	0.873	0.843	0.875	0.849	0.855	0.832	0.776
	LU	TOTAL	0.886	0.857	0.868	0.846	0.837	0.83	0.745
		BKG	0.708	0.665	0.56	0.543	0.522	0.506	0.494
		DIF	0.889	0.843	0.883	0.844	0.835	0.831	0.755
	SEG	TOTAL	0.211	0.215	0.211	0.212	0.21	0.209	0.213
		BKG	0.336	0.336	0.335	0.335	0.335	0.336	0.335
		DIF	0.216	0.217	0.217	0.217	0.217	0.22	0.215

doi:10.6342/NTU202202826

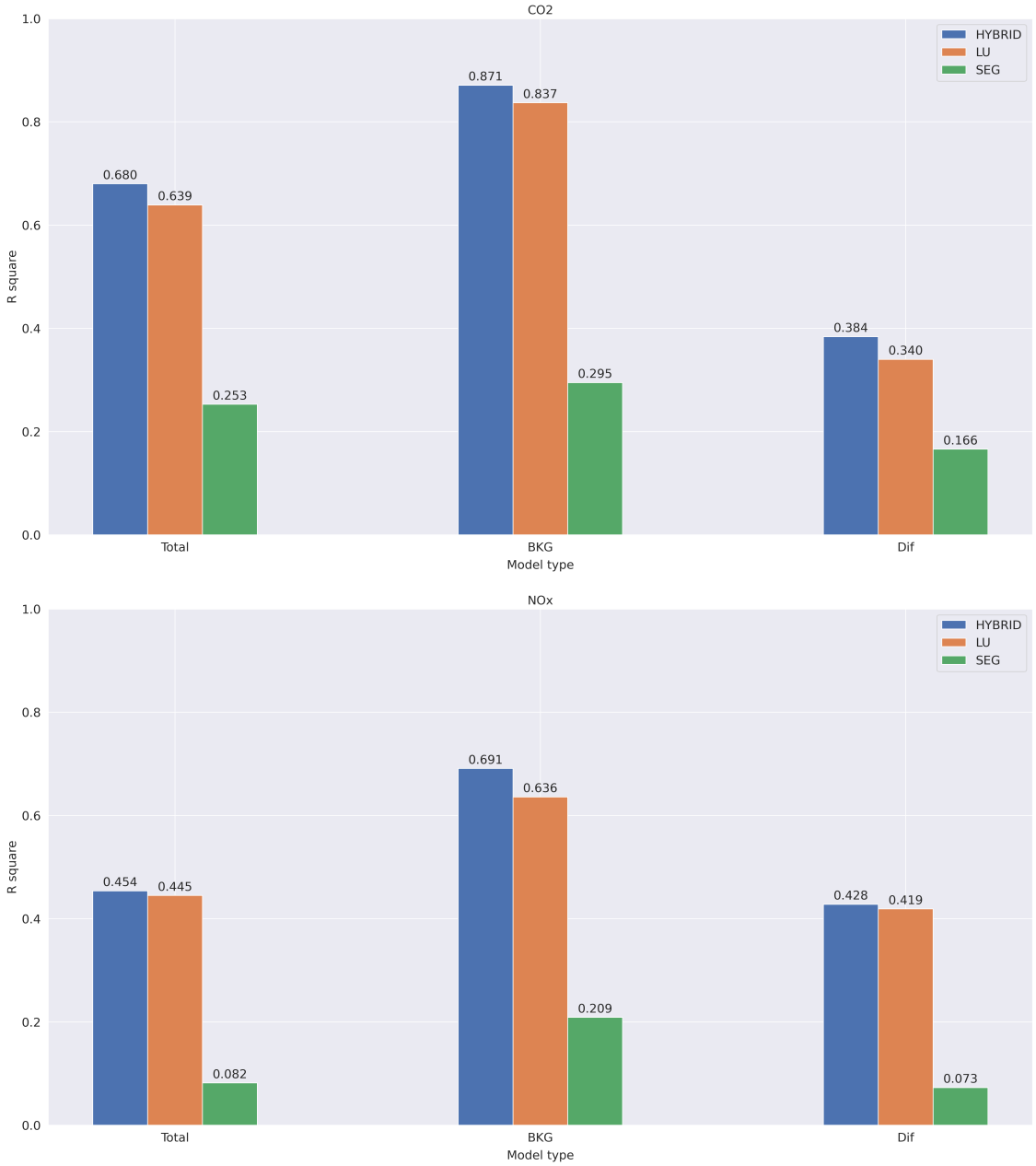

Figure 4.10: HYBRID model without transfer learning 5-fold CV R^2 for the buffer size 700m (1/2)

doi:10.6342/NTU202202826

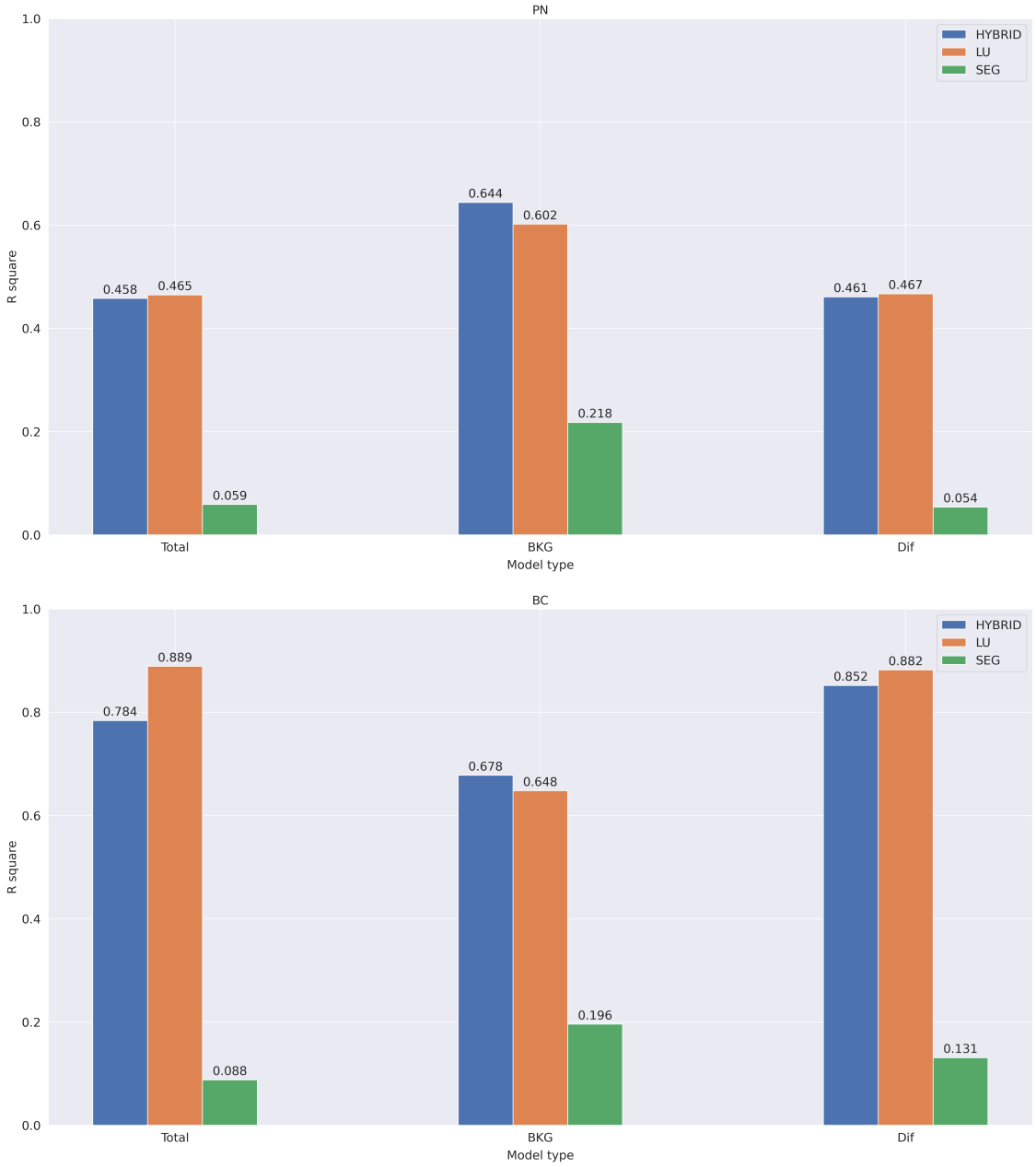

Figure 4.11: HYBRID model without transfer learning 5-fold CV R^2 for the buffer size 700m (2/2)

doi:10.6342/NTU202202826

Table 4.2: R^2 of random sample method without transfer learning

Pollutants	Model types	Concentration types	Buffer size (m)						
			700	600	500	400	300	200	100
CO_2	HYBRID	TOTAL	0.68	0.668	0.656	0.652	0.65	0.65	0.649
		BKG	0.871	0.863	0.856	0.852	0.852	0.852	0.853
		DIF	0.384	0.364	0.344	0.336	0.333	0.335	0.333
	LU	TOTAL	0.639	0.622	0.586	0.579	0.574	0.572	0.564
		BKG	0.837	0.824	0.801	0.795	0.792	0.791	0.79
		DIF	0.34	0.314	0.264	0.253	0.242	0.239	0.226
	SEG	TOTAL	0.253	0.252	0.252	0.253	0.253	0.252	0.252
		BKG	0.295	0.295	0.295	0.295	0.295	0.295	0.295
		DIF	0.166	0.166	0.166	0.166	0.166	0.166	0.166
NOx	HYBRID	TOTAL	0.454	0.411	0.436	0.394	0.392	0.384	0.361
		BKG	0.691	0.671	0.669	0.653	0.646	0.641	0.631
		DIF	0.428	0.381	0.406	0.36	0.357	0.35	0.331
	LU	TOTAL	0.445	0.389	0.387	0.346	0.349	0.342	0.302
		BKG	0.636	0.61	0.6	0.581	0.571	0.564	0.551
		DIF	0.419	0.36	0.359	0.314	0.315	0.309	0.27
	SEG	TOTAL	0.082	0.082	0.082	0.082	0.081	0.081	0.081
		BKG	0.209	0.209	0.209	0.209	0.209	0.209	0.209
		DIF	0.073	0.073	0.072	0.072	0.072	0.073	0.073
PN	HYBRID	TOTAL	0.458	0.404	0.411	0.368	0.364	0.341	0.333
		BKG	0.644	0.609	0.578	0.56	0.559	0.558	0.557
		DIF	0.461	0.406	0.413	0.366	0.364	0.342	0.333
	LU	TOTAL	0.465	0.394	0.38	0.335	0.331	0.313	0.305
		BKG	0.602	0.559	0.489	0.467	0.46	0.456	0.455
		DIF	0.467	0.392	0.38	0.332	0.328	0.311	0.301
	SEG	TOTAL	0.059	0.06	0.06	0.06	0.06	0.06	0.06
		BKG	0.218	0.218	0.218	0.218	0.218	0.218	0.218
		DIF	0.054	0.053	0.053	0.053	0.053	0.053	0.053
BC	HYBRID	TOTAL	0.784	0.742	0.796	0.744	0.751	0.719	0.65
		BKG	0.678	0.648	0.617	0.6	0.589	0.586	0.585
		DIF	0.852	0.814	0.856	0.828	0.835	0.808	0.735
	LU	TOTAL	0.889	0.858	0.883	0.859	0.859	0.849	0.781
		BKG	0.648	0.61	0.553	0.535	0.518	0.509	0.501
		DIF	0.882	0.848	0.875	0.848	0.847	0.834	0.746
	SEG	TOTAL	0.088	0.086	0.086	0.086	0.086	0.086	0.087
		BKG	0.196	0.195	0.196	0.196	0.196	0.195	0.196
		DIF	0.131	0.134	0.134	0.133	0.132	0.131	0.135

doi:10.6342/NTU202202826

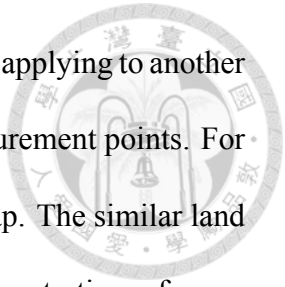

mance in our test case. However, it might cause some overfitting when applying to another dataset. The larger buffer size leads to the overlapping between measurement points. For the model, it was training with similar land use data because of overlap. The similar land use data increases the overfitting effect, especially for smoother concentrations, for example, CO_2 and BKG model. A proper buffer size needs to consider the time resolution of measurements and the speed of the mobile monitoring vehicle. However, our results differ from the previous work. Liu et al. [43] showed their LURF model performance at different smoothing times at different buffer sizes from 25 to 2000 meters. Their highest score is at 25 meters, which is different from our results. We think the difference is from the number of predictor variables. We have more predictor variables that can provide more information to the land use model. This make our land use model more powerful.

Our segmentation model extracts twenty categories from the imagery. The segmentation was trained with transferred images. Transfer learning increases the model performance, as shown in Figure 4.10, Figure 4.11 and 4.2, which is the prediction R^2 of the model using segmentation variables without transfer learning. All models have identical patterns except the decreasing performance. However, transfer learning helps the hybrid model but is not very effective. The old transfer learning model we use might be a problem. Transfer learning cannot guarantee a high-performance increase after transferring. Transfer learning reduces the human effort in processing data. The performance is decided by the quality and quantity of data, segmentation model, transfer learning method, and randomness. Transfer learning is better than directly applying the segmentation model to a dataset without fine-tuning. If we want to enhance the usability of the concentration predicting model, we can collect more data and experiment with other transfer learning methods and segmentation models.

doi:10.6342/NTU202202826

4.4 One-day method

To investigate the possibility of applying the hybrid model to actual applications, we conducted experiments with the hybrid model in a different data-splitting method. The concentration data were measured over eight days. We assume there isn't any relation between days. We can select one day as testing data and the others as training data, which is like an 8-fold cross-validation. As shown in Figure 4.12, Figure 4.13 and 4.3, the model performance is worse than the random sample results—the R^2 of all combinations decreases. Although the BKG is still better than the other two, changing the data-splitting method dramatically impacts the model performance. The concentration data has time continuity. When we measure the concentration in a short time resolution like two seconds, the measurements don't directly jump to another value. Suppose we use the random sample method to split the data for training and testing. In that case, the model using training data already knows the answer before and after the specific testing data. It causes misjudgment about the model's performance. This problem is related to the limitation of concentration data. The model is easy to overfit on concentration data with a high time resolution using the random sample method because of the continuity of data.

As for the one-day method, we think it is a better method to evaluate a model. However, the data variance between days and lack of time information during measuring decrease the model's performance. Predictor variables don't have enough info besides the LU and SEG for the model to predict the concentration of another day. Increasing the quantity of data to cover any situation that causes the variance makes the model evaluation more reliable. We believe that the one-day method will eventually have the same performance as the random sample method. As for the results of the one-day method with-

doi:10.6342/NTU202202826

out transfer learning, we think the results with transfer learning so far already show worse performance than the random sample method, so we only test the one-day method with transfer learning.

Figure 4.12: HYBRID model with one-day method 5-fold CV R^2 for the buffer size 700m (1/2)

doi:10.6342/NTU202202826

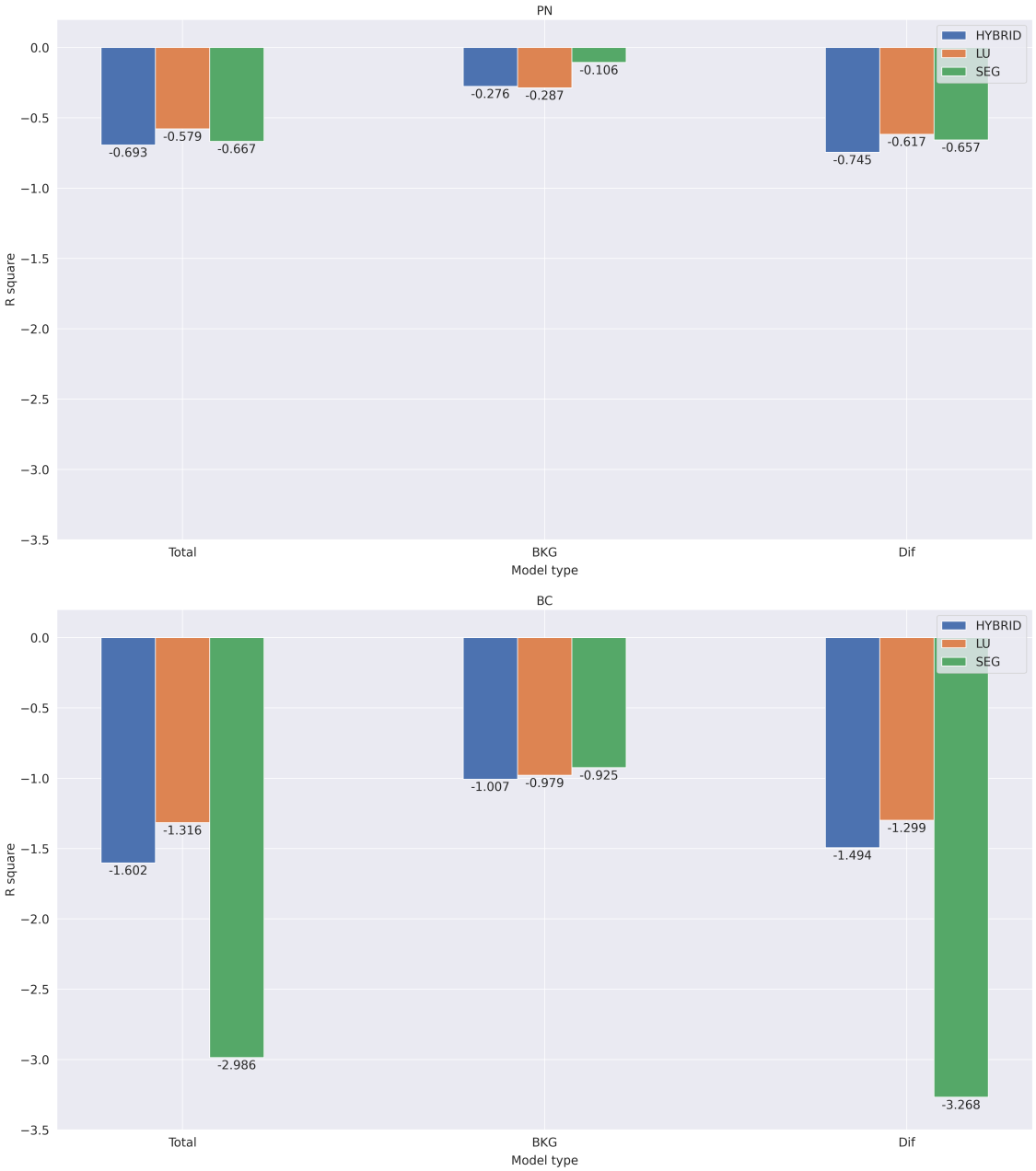

Figure 4.13: HYBRID model with one-day method 5-fold CV R^2 for the buffer size 700m (2/2)

doi:10.6342/NTU202202826

Table 4.3: R^2 of one-day method with transfer learning

Pollutants	Model types	Concentration types	Buffer size (m)						
			700	600	500	400	300	200	100
CO_2	HYBRID	TOTAL	0.085	0.084	0.065	0.063	0.057	0.058	0.062
		BKG	-0.007	-0.074	-0.011	-0.062	-0.072	-0.077	-0.076
		DIF	-0.02	-0.031	-0.069	-0.065	-0.072	-0.07	-0.068
	LU	TOTAL	0.042	0.043	0.02	0.026	0.022	0.018	0.024
		BKG	-0.081	-0.143	-0.144	-0.175	-0.172	-0.162	-0.164
		DIF	-0.036	-0.05	-0.072	-0.075	-0.092	-0.095	-0.08
	SEG	TOTAL	-0.316	-0.318	-0.317	-0.316	-0.318	-0.316	-0.316
		BKG	-1.121	-1.12	-1.124	-1.119	-1.119	-1.118	-1.125
		DIF	-0.096	-0.094	-0.094	-0.094	-0.094	-0.095	-0.094
NOx	HYBRID	TOTAL	-0.197	-0.04	-0.191	-0.06	-0.043	-0.038	-0.057
		BKG	-0.223	-0.121	-0.203	-0.101	-0.097	-0.098	-0.098
		DIF	-0.222	-0.055	-0.209	-0.074	-0.06	-0.054	-0.072
	LU	TOTAL	-0.178	-0.033	-0.117	-0.024	-0.011	-0.008	-0.019
		BKG	-0.269	-0.197	-0.205	-0.113	-0.135	-0.127	-0.136
		DIF	-0.185	-0.047	-0.119	-0.036	-0.021	-0.017	-0.026
	SEG	TOTAL	-0.375	-0.375	-0.378	-0.371	-0.372	-0.374	-0.373
		BKG	-2.386	-2.382	-2.381	-2.391	-2.384	-2.387	-2.384
		DIF	-0.302	-0.296	-0.299	-0.295	-0.3	-0.3	-0.3
PN	HYBRID	TOTAL	-0.693	-0.362	-0.604	-0.365	-0.349	-0.352	-0.355
		BKG	-0.276	-0.28	-0.318	-0.314	-0.32	-0.322	-0.324
		DIF	-0.745	-0.366	-0.643	-0.339	-0.326	-0.344	-0.331
	LU	TOTAL	-0.579	-0.28	-0.435	-0.266	-0.25	-0.246	-0.245
		BKG	-0.287	-0.29	-0.358	-0.355	-0.361	-0.354	-0.354
		DIF	-0.617	-0.265	-0.453	-0.244	-0.222	-0.227	-0.224
	SEG	TOTAL	-0.667	-0.671	-0.672	-0.667	-0.67	-0.669	-0.667
		BKG	-0.106	-0.107	-0.106	-0.105	-0.106	-0.104	-0.107
		DIF	-0.657	-0.654	-0.652	-0.66	-0.652	-0.646	-0.658
BC	HYBRID	TOTAL	-1.602	-0.834	-1.807	-0.929	-0.639	-0.696	-0.758
		BKG	-1.007	-1.043	-1.042	-1.031	-1.022	-1.025	-1.034
		DIF	-1.494	-0.696	-1.465	-0.759	-0.532	-0.584	-0.649
	LU	TOTAL	-1.316	-0.872	-1.198	-0.51	-0.37	-0.313	-0.305
		BKG	-0.979	-1.005	-1.033	-1.002	-0.99	-0.997	-0.98
		DIF	-1.299	-0.72	-1.048	-0.45	-0.337	-0.277	-0.285
	SEG	TOTAL	-2.986	-2.989	-2.926	-2.909	-2.981	-3.05	-2.98
		BKG	-0.925	-0.924	-0.926	-0.927	-0.926	-0.924	-0.924
		DIF	-3.268	-3.277	-3.174	-3.308	-3.191	-3.272	-3.15

doi:10.6342/NTU202202826

Chapter 5 CONCLUSION

Our study has some contributions and limitations. We show them in three different parts to match our objective. The first is about the machine learning model. Next is our model performance and ability. The Final is the settings of land use random forest.

5.1 Flexibility of the image segmentation model

We introduce the transfer learning model to reduce the human work of processing data. We can extract features from low-resolution unlabeled imagery. We do not need to manually label our training data because of transfer learning and use an open-source dataset to achieve good performance in predicting pollutants concentration. Increasing R^2 of CO_2, NOx, PN, and BC concentrations from 0.68, 0.45, 0.46, and 0.78 to 0.79, 0.63, 0.61, and 0.88, respectively. We reach similar performance without labeling and GSV data compared to previous works [33, 34, 38, 53, 54]. However, our transfer learning method is not state-of-the-art, and the segmentation model is not as well. Many models can increase transfer learning performance. However, the transfer learning and segmentation model also create errors during the feature-extracting procedure. This factor, along with the lack of quantity and quality of image data, affects the SEG model performance. Future work could apply our approach to another dataset that has enough data. This approach can also apply to the region where there is a lack of GSV imagery.

doi:10.6342/NTU202202826

5.2 Spatiotemporal variability

We introduce a random forest model that can well predict pollutants concentrations. The model explains 80, 90, 60, and 60 percent of the CO_2, NOx, PN, and BC concentration variability, respectively. Our results also demonstrated the characteristics of different pollutants. SEG model shows the various performances of various pollutants and concentration types. SEG model can provide the temporal information that the LU model does not have. It helps the LU model to predict CO_2, NOx, and PN. However, it needs more temporal information to help BC or even help the one-day method.

5.3 The settings of land use random forest

We apply the land use random forest to estimate the pollutant concentrations. Sensitivity analysis of buffer size shows that 500 m is more balance for the land use variables. We also compared two different methods for splitting training and testing data. Apparently, our models do not have enough temporal information for predicting one day, and it leads to the lower R^2 of the one-day method. However, we cannot conclude which method is better, it depends on the purpose of splitting data. In our opinion, the limitation here is the concentration data itself. The characteristic of concentration data affects the model performance depending on how we select testing data. Future work could collect more data to reduce the effect caused by data. More data can probably solve the variance problem.

Our study shows the potential of the transfer learning model in estimating pollutant concentrations. It can apply to any onboard camera or any weather. A large amount of road source emissions can be calculated at a low cost. GPS and a camera can estimate

doi:10.6342/NTU202202826

pollutant concentrations without labeling data. This is useful for the region inaccessible for the mobile monitoring vehicle or where there is no GSV data. As cheap sensors, intersection monitors, and onboard cameras are more and more common, the combination of street-level image analysis and mobile monitoring has become a new trend in estimating air pollution exposure at the small spatiotemporal level. Transfer learning can help reduce costs and make it easier to apply anywhere in the world.

doi:10.6342/NTU202202826

References

[1] Ibon Eguiluz-Gracia, Alexander G. Mathioudakis, Sabine Bartel, Susanne J.H. Vijverberg, Elaine Fuertes, Pasquale Comberiati, Yutong Samuel Cai, Peter Valentin Tomazic, Zuzana Diamant, Jørgen Vestbo, Carmen Galan, and Barbara Hoffmann. The need for clean air: The way air pollution and climate change affect allergic rhinitis and asthma. Allergy: European Journal of Allergy and Clinical Immunology, 75, 2020.

[2] Haidong Kan, Renjie Chen, and Shilu Tong. Ambient air pollution, climate change, and population health in china. Environment International, 42, 2012.

[3] Intergovernmental Panel on Climate Change. Ipcc’s sixth assessment report, 2021.

[4] C. Arden Pope, Majid Ezzati, and Douglas W. Dockery. Fine-particulate air pollution and life expectancy in the united states. New England Journal of Medicine, 360, 2009.

[5] Gerard Hoek, Ranjini M. Krishnan, Rob Beelen, Annette Peters, Bart Ostro, Bert Brunekreef, and Joel D. Kaufman. Long-term air pollution exposure and cardio-respiratory mortality: A review. Environmental Health: A Global Access Science Source, 12, 2013.

[6] Ki Hyun Kim, Ehsanul Kabir, and Shamin Kabir. A review on the human health impact of airborne particulate matter. Environment International, 74, 2015.

[7] Zhenyu Luo, Yue Wang, Zhaofeng Lv, Tingkun He, Junchao Zhao, Yongyue Wang,

doi:10.6342/NTU202202826

Fei Gao, Zhining Zhang, and Huan Liu. Impacts of vehicle emission on air quality and human health in china. Science of the Total Environment, 813, 2022.

[8] Frank J. Kelly and Julia C. Fussell. Air pollution and public health: emerging hazards and improved understanding of risk. Environmental Geochemistry and Health, 37, 2015.

[9] Dai Hua Tsai, Yi Her Wu, and Chang Chuan Chan. Comparisons of commuter's exposure to particulate matters while using different transportation modes. Science of the Total Environment, 405, 2008.

[10] Tran Ngoc Quang, Nguyen Thi Hue, Mac Van Dat, Long K. Tran, Thai Ha Phi, Lidia Morawska, and Phong K. Thai. Motorcyclists have much higher exposure to black carbon compared to other commuters in traffic of hanoi, vietnam. Atmospheric Environment, 245, 2021.

[11] Hsien Chih Li, Pei Te Chiueh, Shi Ping Liu, and Yu Yang Huang. Assessment of different route choice on commuters' exposure to air pollution in taipei, taiwan. Environmental Science and Pollution Research, 24, 2017.

[12] Joshua S. Apte, Kyle P. Messier, Shahzad Gani, Michael Brauer, Thomas W. Kirchstetter, Melissa M. Lunden, Julian D. Marshall, Christopher J. Portier, Roel C.H. Vermeulen, and Steven P. Hamburg. High-resolution air pollution mapping with google street view cars: Exploiting big data. Environmental Science and Technology, 51, 2017.

[13] David J. Miller, Blake Actkinson, Lauren Padilla, Robert J. Griffin, Katie Moore, P. Grace Tee Lewis, Rivkah Gardner-Frolick, Elena Craft, Christopher J. Portier,

doi:10.6342/NTU202202826

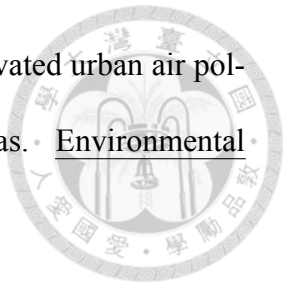

Steven P. Hamburg, and Ramón A. Alvarez. Characterizing elevated urban air pollutant spatial patterns with mobile monitoring in houston, texas. Environmental Science and Technology, 54, 2020.

[14] Stacey E. Alexeeff, Ananya Roy, Jun Shan, Xi Liu, Kyle Messier, Joshua S. Apte, Christopher Portier, Stephen Sidney, and Stephen K. Van Den Eeden. High-resolution mapping of traffic related air pollution with google street view cars and incidence of cardiovascular events within neighborhoods in oakland, ca. Environmental Health: A Global Access Science Source, 17, 2018.

[15] Timothy Larson, Sarah B. Henderson, and Michael Brauer. Mobile monitoring of particle light absorption coefficient in an urban area as a basis for land use regression. Environmental Science and Technology, 43, 2009.

[16] Paul A. Solomon, Dennis Crumpler, James B. Flanagan, R. K.M. Jayanty, Ed E. Rickman, and Charles E. McDade. U.s. national pm2.5 chemical speciation monitoring networks—csn and improve: Description of networks. Journal of the Air and Waste Management Association, 64, 2014.

[17] Prashant Kumar, Lidia Morawska, Claudio Martani, George Biskos, Marina Neophytou, Silvana Di Sabatino, Margaret Bell, Leslie Norford, and Rex Britter. The rise of low-cost sensing for managing air pollution in cities. Environment International, 75, 2015.

[18] Laura Minet, Rick Liu, Marie France Valois, Junshi Xu, Scott Weichenthal, and Marianne Hatzopoulou. Development and comparison of air pollution exposure surfaces derived from on-road mobile monitoring and short-term stationary sidewalk measurements. Environmental Science and Technology, 52, 2018.

doi:10.6342/NTU202202826

[19] Yanju Chen, Peishi Gu, Nico Schulte, Xiaochi Zhou, Steve Mara, Bart E. Croes, Jorn D. Herner, and Abhilash Vijayan. A new mobile monitoring approach to characterize community-scale air pollution patterns and identify local high pollution zones. Atmospheric Environment, 272, 2022.

[20] Lauren E. Padilla, Geoffrey Q. Ma, Daniel Peters, Megan Dupuy-Todd, Ella Forsyth, Amy Stidworthy, Jim Mills, Stefan Bell, Idris Hayward, Georgie Coppin, Katie Moore, Elizabeth Fonseca, Olalekan A.M. Popoola, Felicia Douglas, Greg Slater, Karin Tuxen-Bettman, David Carruthers, Nicholas A. Martin, Roderic L. Jones, and Ramón A. Alvarez. New methods to derive street-scale spatial patterns of air pollution from mobile monitoring. Atmospheric Environment, 270, 2022.

[21] Marloes Eeftens, Rob Beelen, Kees De Hoogh, Tom Bellander, Giulia Cesaroni, Marta Cirach, Christophe Declercq, Audrius Dedele, Evi Dons, Audrey De Nazelle, Konstantina Dimakopoulou, Kirsten Eriksen, Grégoire Falq, Paul Fischer, Claudia Galassi, Regina Gražulevičiene, Joachim Heinrich, Barbara Hoffmann, Michael Jerrett, Dirk Keidel, Michal Korek, Timo Lanki, Sarah Lindley, Christian Madsen, Anna Mölter, Gizella Nádor, Mark Nieuwenhuijsen, Michael Nonnemacher, Xanthi Pedeli, Ole Raaschou-Nielsen, Evridiki Patelarou, Ulrich Quass, Andrea Ranzi, Christian Schindler, Morgane Stempfelet, Euripides Stephanou, Dorothea Sugiri, Ming Yi Tsai, Tarja Yli-Tuomi, Mihály J. Varró, Danielle Vienneau, Stephanie Von Klot, Kathrin Wolf, Bert Brunekreef, and Gerard Hoek. Development of land use regression models for pm2.5, pm 2.5 absorbance, pm10 and pmcoarse in 20 european study areas; results of the escape project. Environmental Science and Technology, 46, 2012.

[22] Oliver Schmitz, Rob Beelen, Maciej Strak, Gerard Hoek, Ivan Soenario, Bert

doi:10.6342/NTU202202826

Brunekreef, Ilonca Vaartjes, Martin J. Dijst, Diederick E. Grobbee, and Derek Karssenberg. Data descriptor: High resolution annual average air pollution concentration maps for the netherlands. Scientific Data, 6, 2019.

[23] Andrew Larkin, Jeffrey A. Geddes, Randall V. Martin, Qingyang Xiao, Yang Liu, Julian D. Marshall, Michael Brauer, and Perry Hystad. Global land use regression model for nitrogen dioxide air pollution. Environmental Science and Technology, 51, 2017.

[24] Hyung Joo Lee. Benefits of high resolution pm2.5 prediction using satellite maiac aod and land use regression for exposure assessment: California examples. Environmental Science and Technology, 53, 2019.

[25] Xiaomeng Wu, Daoyuan Yang, Ruoxi Wu, Jiajun Gu, Yifan Wen, Shaojun Zhang, Rui Wu, Renjie Wang, Honglei Xu, K. Max Zhang, Ye Wu, and Jiming Hao. High-resolution mapping of regional traffic emissions using land-use machine learning models. Atmospheric Chemistry and Physics, 22, 2022.

[26] Steve Hankey, Peter Sforza, and Matt Pierson. Using mobile monitoring to develop hourly empirical models of particulate air pollution in a rural appalachian community. Environmental Science and Technology, 53, 2019.

[27] Kyle P. Messier, Sarah E. Chambliss, Shahzad Gani, Ramon Alvarez, Michael Brauer, Jonathan J. Choi, Steven P. Hamburg, Jules Kerckhoffs, Brian Lafranchi, Melissa M. Lunden, Julian D. Marshall, Christopher J. Portier, Ananya Roy, Adam A. Szpiro, Roel C.H. Vermeulen, and Joshua S. Apte. Mapping air pollution with google street view cars: Efficient approaches with mobile monitoring and land use regression. Environmental Science and Technology, 52, 2018.

doi:10.6342/NTU202202826

[28] Marianne Hatzopoulou, Marie France Valois, Ilan Levy, Cristian Mihele, Gang Lu, Scott Bagg, Laura Minet, and Jeffrey Brook. Robustness of land-use regression models developed from mobile air pollutant measurements. Environmental Science and Technology, 51, 2017.

[29] Andrew G. Rundle, Michael D.M. Bader, Catherine A. Richards, Kathryn M. Neckerman, and Julien O. Teitler. Using google street view to audit neighborhood environments. American Journal of Preventive Medicine, 40, 2011.

[30] Kees de Hoogh, Michal Korek, Danielle Vienneau, Menno Keuken, Jaakko Kukkonen, Mark J. Nieuwenhuijsen, Chiara Badaloni, Rob Beelen, Andrea Bolignano, Giulia Cesaroni, Marta Cirach Pradas, Josef Cyrys, John Douros, Marloes Eeftens, Francesco Forastiere, Bertil Forsberg, Kateryna Fuks, Ulrike Gehring, Alexandros Gryparis, John Gulliver, Anna L. Hansell, Barbara Hoffmann, Christer Johansson, Sander Jonkers, Leena Kangas, Klea Katsouyanni, Nino Künzli, Timo Lanki, Michael Memmesheimer, Nicolas Moussiopoulos, Lars Modig, Göran Pershagen, Nicole Probst-Hensch, Christian Schindler, Tamara Schikowski, Dorothee Sugiri, Oriol Teixidó, Ming Yi Tsai, Tarja Yli-Tuomi, Bert Brunekreef, Gerard Hoek, and Tom Bellander. Comparing land use regression and dispersion modelling to assess residential exposure to ambient air pollution for epidemiological studies. Environment International, 73, 2014.

[31] Steve Hankey and Julian D. Marshall. Land use regression models of on-road particulate air pollution (particle number, black carbon, pm2.5, particle size) using mobile monitoring. Environmental Science and Technology, 49, 2015.

[32] Jianming Liang, Jianhua Gong, Jun Sun, Jieping Zhou, Wenhang Li, Yi Li, Jin Liu,

doi:10.6342/NTU202202826

and Shen Shen. Automatic sky view factor estimation from street view photographs - a big data approach. Remote Sensing, 9, 2017.

[33] Xiansheng Liu, Hadiatullah Hadiatullah, Xun Zhang, L. Drew Hill, Andrew H.A. White, Jurgen Schnelle-Kreis, Jan Bendl, Gert Jakobi, Brigitte Schloter-Hai, and Ralf Zimmermann. Analysis of mobile monitoring data from the microaeth® ma200 for measuring changes in black carbon on the roadside in augsburg. Atmospheric Measurement Techniques, 14, 2021.

[34] Xiansheng Liu, Xun Zhang, Jürgen Schnelle-Kreis, Gert Jakobi, Xin Cao, Josef Cyrys, Lanyan Yang, Brigitte Schloter-Hai, Gülcin Abbaszade, Jürgen Orasche, Mohamed Khedr, Michal Kowalski, Marcus Hank, and Ralf Zimmermann. Spatiotemporal characteristics and driving factors of black carbon in augsburg, germany: Combination of mobile monitoring and street view images. Environmental Science and Technology, 55, 2021.

[35] Xiaojiang Li, Chuanrong Zhang, Weidong Li, Robert Ricard, Qingyan Meng, and Weixing Zhang. Assessing street-level urban greenery using google street view and a modified green view index. Urban Forestry and Urban Greening, 14, 2015.

[36] Philip Stubbings, Joe Peskett, Francisco Rowe, and Dani Arribas-Bel. A hierarchical urban forest index using street-level imagery and deep learning. Remote Sensing, 11, 2019.

[37] Ian Seiferling, Nikhil Naik, Carlo Ratti, and Raphäel Proulx. Green streets − quantifying and mapping urban trees with street-level imagery and computer vision. Landscape and Urban Planning, 165, 2017.

doi:10.6342/NTU202202826

[38] Meng Qi and Steve Hankey. Using street view imagery to predict street-level particulate air pollution. Environmental Science and Technology, 55, 2021.

[39] Jun Yan Zhu, Taesung Park, Phillip Isola, and Alexei A. Efros. Unpaired image-to-image translation using cycle-consistent adversarial networks. Proceedings of the IEEE International Conference on Computer Vision, 2017-October, 2017.

[40] Liang Chieh Chen, George Papandreou, Iasonas Kokkinos, Kevin Murphy, and Alan L. Yuille. Deeplab: Semantic image segmentation with deep convolutional nets, atrous convolution, and fully connected crfs. IEEE Transactions on Pattern Analysis and Machine Intelligence, 40, 2018.

[41] Arman Ganji, Laura Minet, Scott Weichenthal, and Marianne Hatzopoulou. Predicting traffic-related air pollution using feature extraction from built environment images. Environmental Science and Technology, 54, 2020.

[42] Amanda Rzotkiewicz, Amber L. Pearson, Benjamin V. Dougherty, Ashton Shortridge, and Nick Wilson. Systematic review of the use of google street view in health research: Major themes, strengths, weaknesses and possibilities for future research. Health and Place, 52, 2018.

[43] Xiansheng Liu, Hadiatullah Hadiatullah, Xun Zhang, Jürgen Schnelle-Kreis, Xiaohu Zhang, Xiuxiu Lin, Xin Cao, and Ralf Zimmermann. Combined land-use and street view image model for estimating black carbon concentrations in urban areas. Atmospheric Environment, 265, 2021.

[44] Douglas Aaron and Costas Tsouris. Separation of co2 from flue gas: A review. Separation Science and Technology, 40, 2005.

doi:10.6342/NTU202202826

[45] Colleen E. Reid, Michael Jerrett, Maya L. Petersen, Gabriele G. Pfister, Philip E. Morefield, Ira B. Tager, Sean M. Raffuse, and John R. Balmes. Spatiotemporal prediction of fine particulate matter during the 2008 northern california wildfires using machine learning. Environmental Science and Technology, 49, 2015.

[46] Qian Di, Itai Kloog, Petros Koutrakis, Alexei Lyapustin, Yujie Wang, and Joel Schwartz. Assessing pm2.5 exposures with high spatiotemporal resolution across the continental united states. Environmental Science and Technology, 50, 2016.

[47] Xuefei Hu, Jessica H. Belle, Xia Meng, Avani Wildani, Lance A. Waller, Matthew J. Strickland, and Yang Liu. Estimating pm2.5 concentrations in the conterminous united states using the random forest approach. Environmental Science and Technology, 51, 2017.

[48] Cole Brokamp, Roman Jandarov, M. B. Rao, Grace LeMasters, and Patrick Ryan. Exposure assessment models for elemental components of particulate matter in an urban environment: A comparison of regression and random forest approaches. Atmospheric Environment, 151, 2017.

[49] Cole Brokamp, Roman Jandarov, Monir Hossain, and Patrick Ryan. Predicting daily urban fine particulate matter concentrations using a random forest model. Environmental Science and Technology, 52, 2018.

[50] Leo Breiman. Bagging predictors. Machine Learning, 24, 1996.

[51] Tin Kam Ho. The random subspace method for constructing decision forests. IEEE Transactions on Pattern Analysis and Machine Intelligence, 20, 1998.

[52] Jih-Hsun Yeh. 對移動污染源及固定污染源的排放強度進行估計: 以實際道路

doi:10.6342/NTU202202826

車隊及工業區料堆爲例. 臺灣大學環境工程學研究所學位論文, pages 1–100, 1 2021.

[53] Sheila Tripathy, Brett J. Tunno, Drew R. Michanowicz, Ellen Kinnee, Jessie L.C. Shmool, Sara Gillooly, and Jane E. Clougherty. Hybrid land use regression modeling for estimating spatio-temporal exposures to pm 2.5 , bc, and metal components across a metropolitan area of complex terrain and industrial sources. Science of the Total Environment, 673, 2019.

[54] Marshall Lloyd, Ellison Carter, Florencio Guzman Diaz, Kento Taro Magara-Gomez, Kris Y. Hong, Jill Baumgartner, Víctor M. Herrera G, and Scott Weichenthal. Predicting within-city spatial variations in outdoor ultrafine particle and black carbon concentrations in bucaramanga, colombia: A hybrid approach using open-source geographic data and digital images. Environmental Science and Technology, 55, 2021.

doi:10.6342/NTU202202826

Appendix A — Regression results

doi:10.6342/NTU202202826

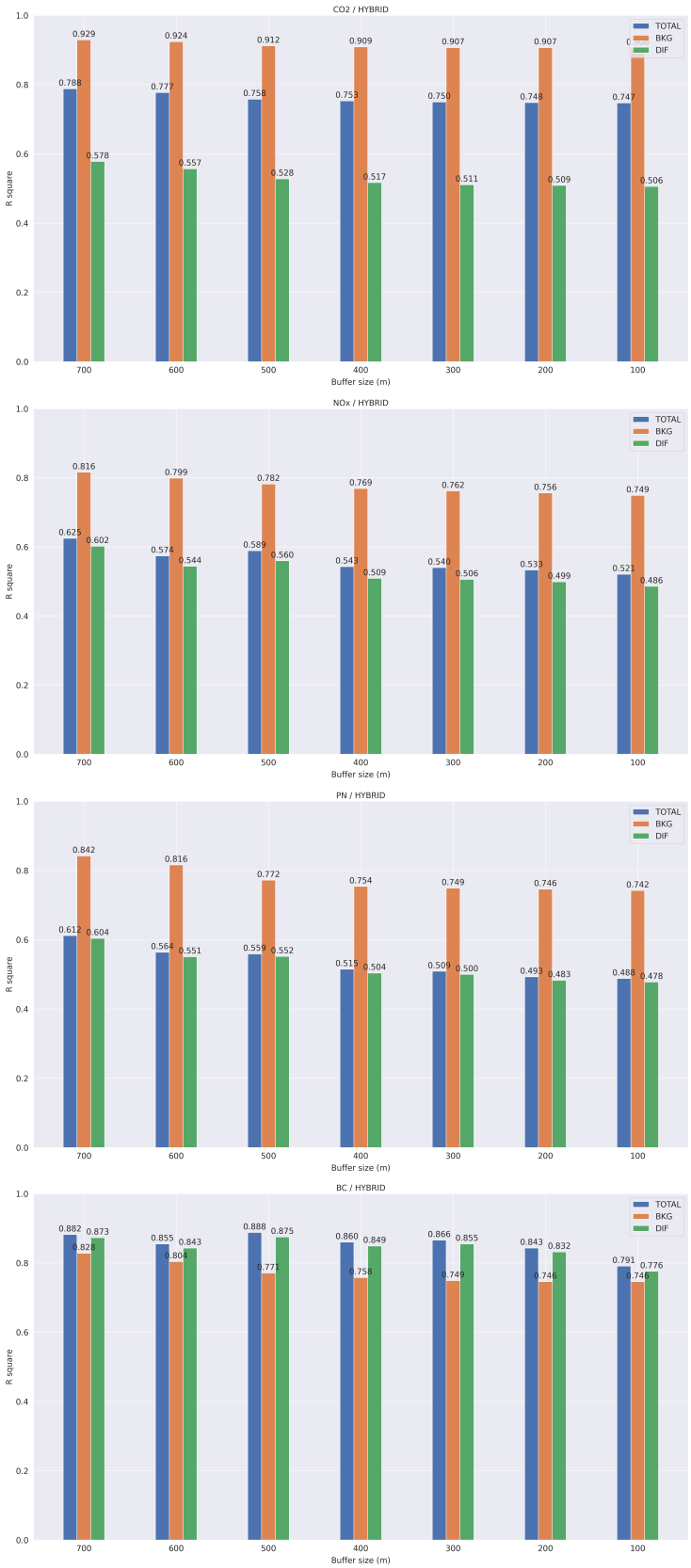

Figure A.1: HYBRID model sensitivity analysis of buffer size (Random sample with transfer learning)

doi:10.6342/NTU202202826

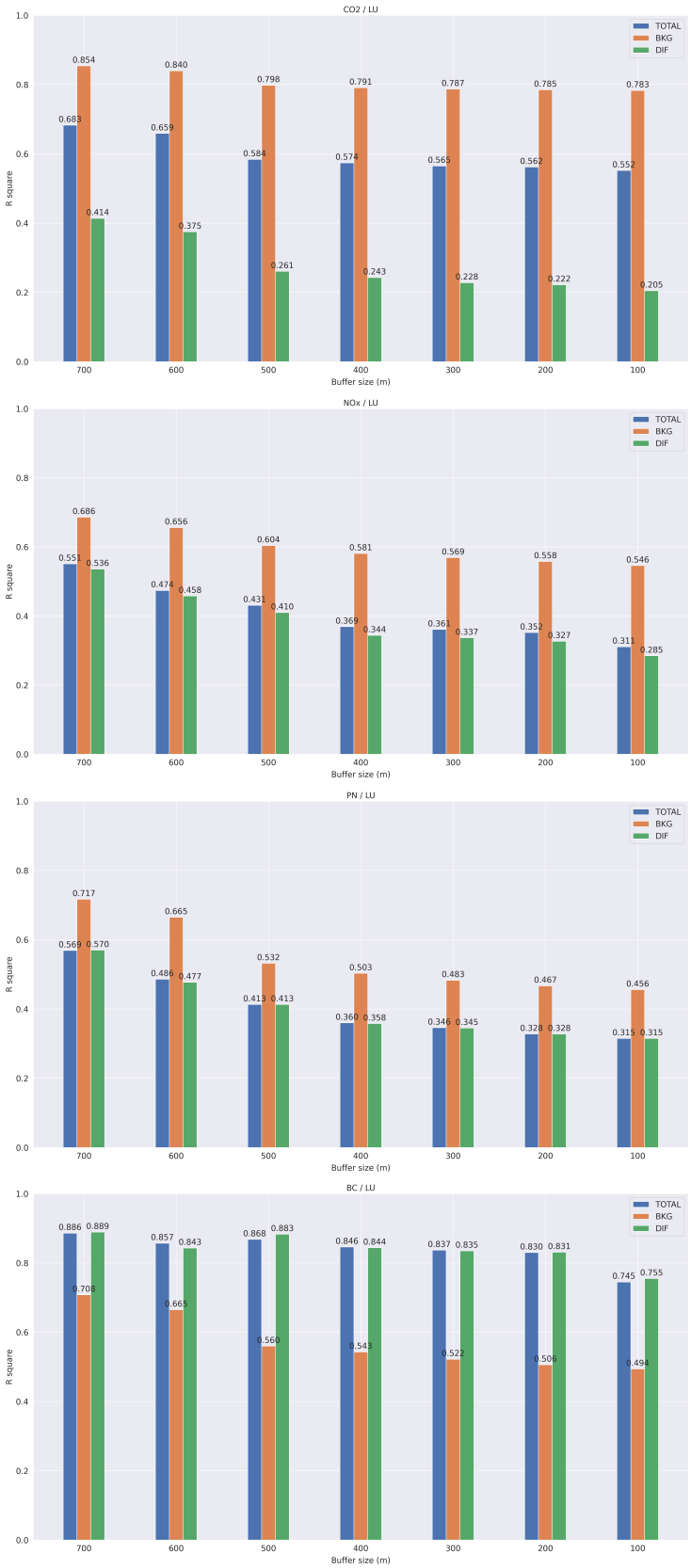

Figure A.2: LU model sensitivity analysis of buffer size (Random sample with transfer learning)

doi:10.6342/NTU202202826

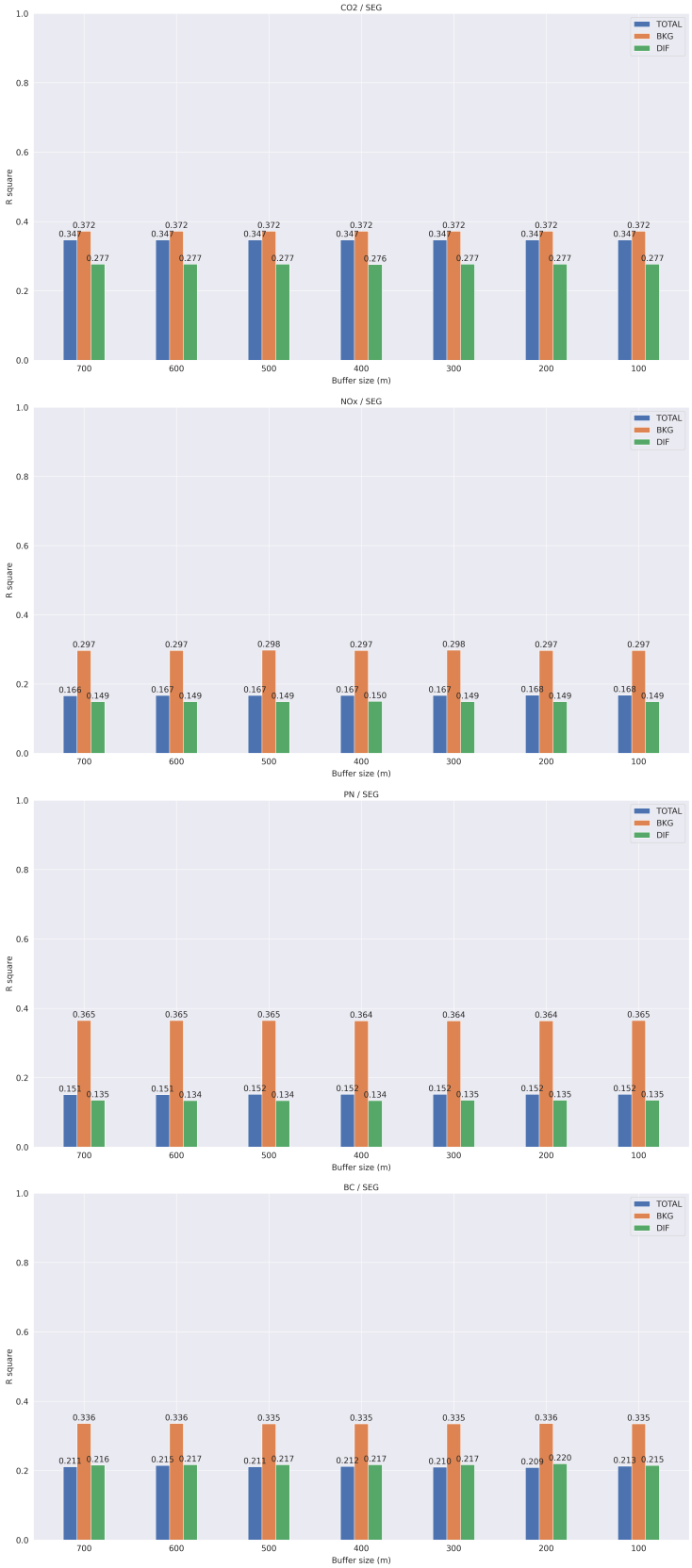

Figure A.3: SEG model sensitivity analysis of buffer size (Random sample with transfer learning)

doi:10.6342/NTU202202826

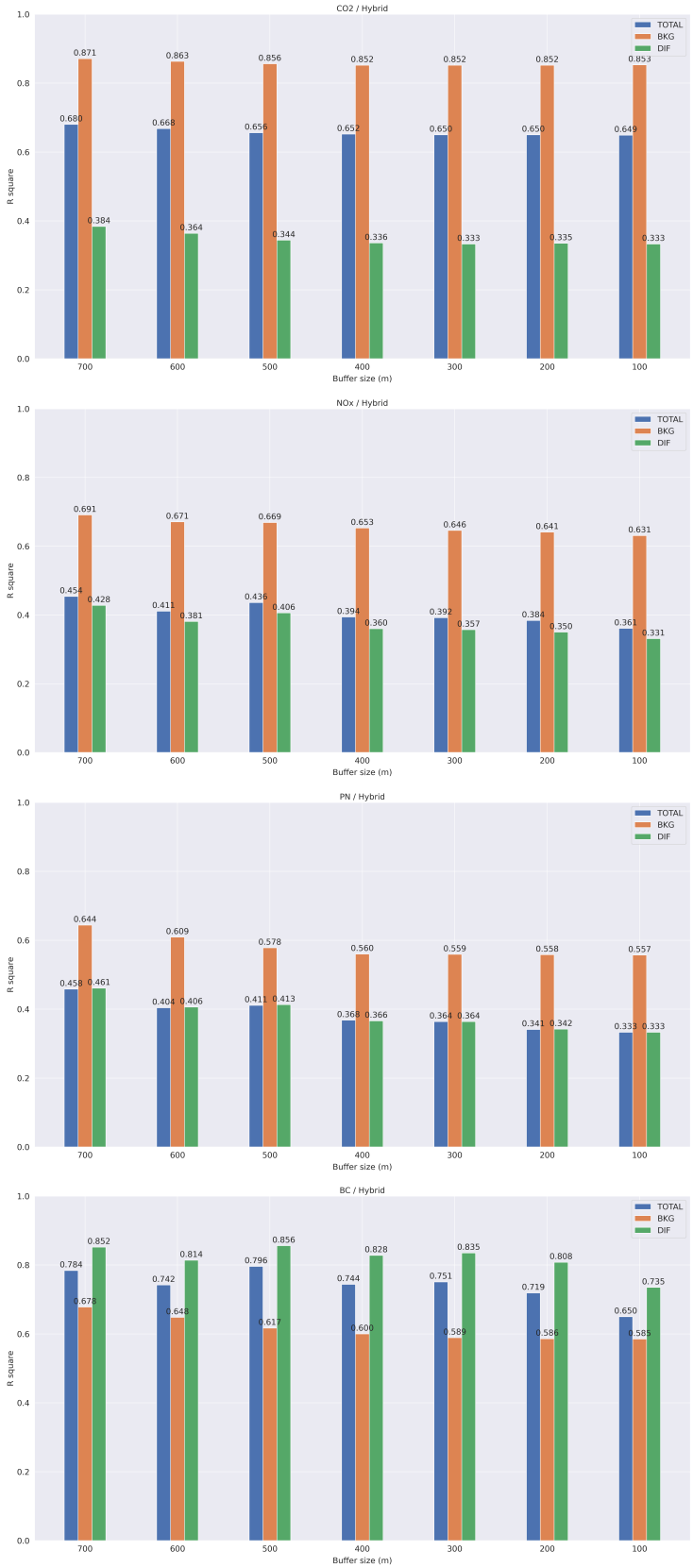

Figure A.4: HYBRID model sensitivity analysis of buffer size (Random sample without transfer learning)

doi:10.6342/NTU202202826

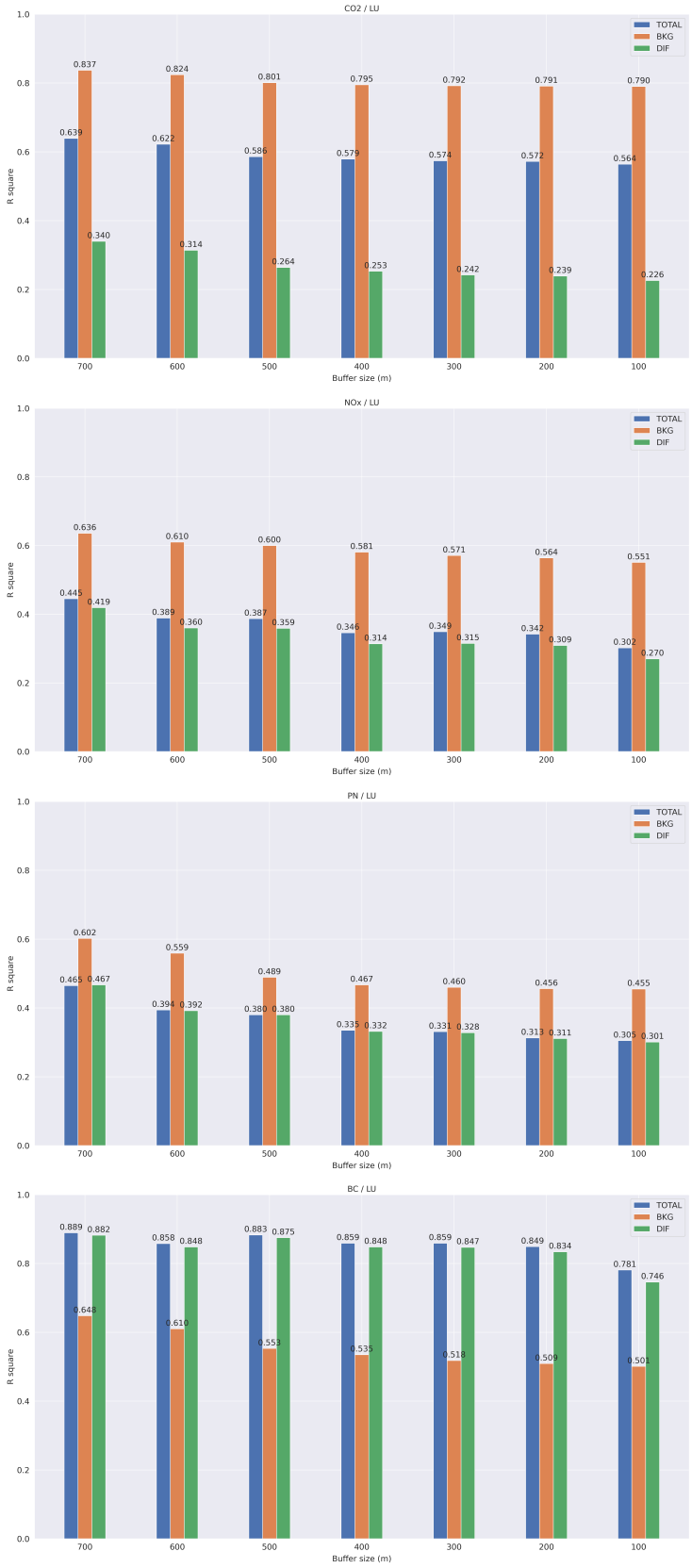

Figure A.5: LU model sensitivity analysis of buffer size (Random sample without transfer learning)

doi:10.6342/NTU202202826

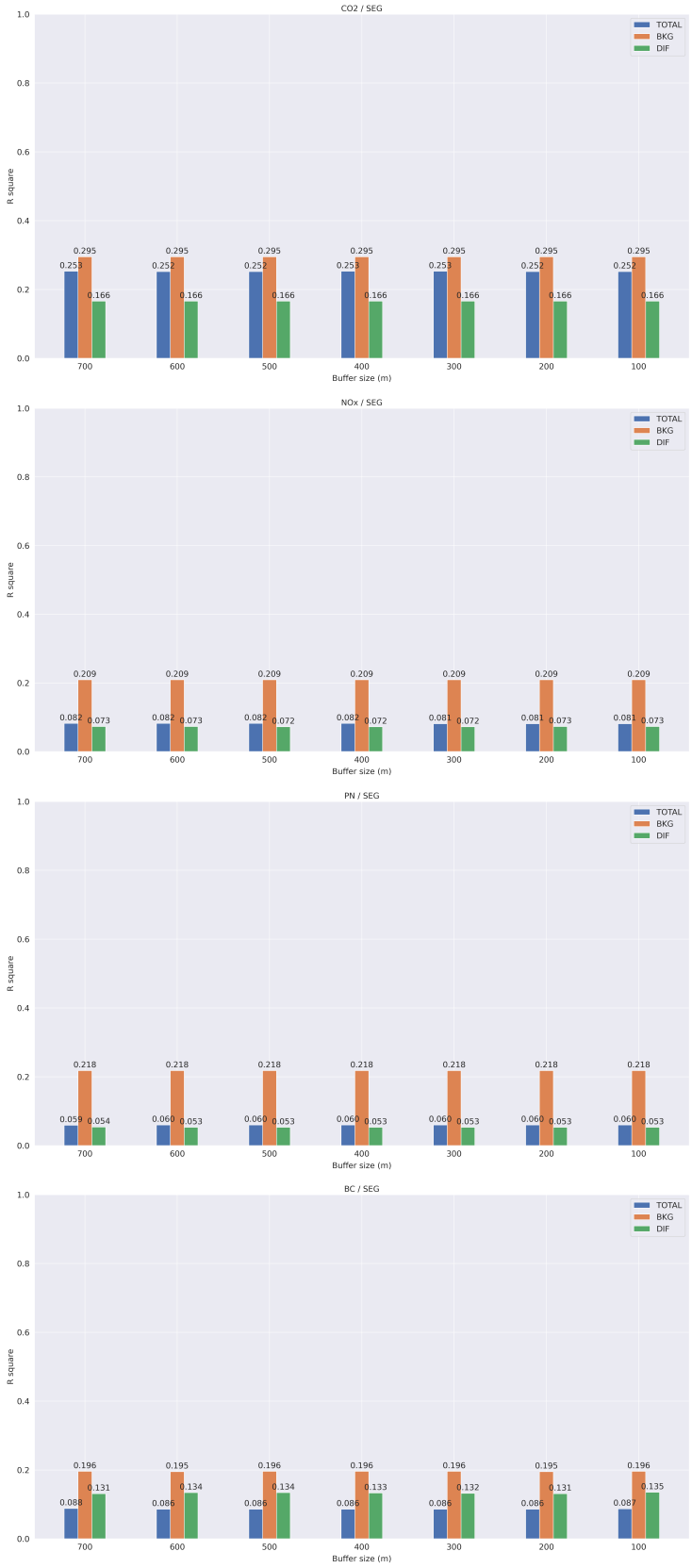

Figure A.6: SEG model sensitivity analysis of buffer size (Random sample without transfer learning)

doi:10.6342/NTU202202826

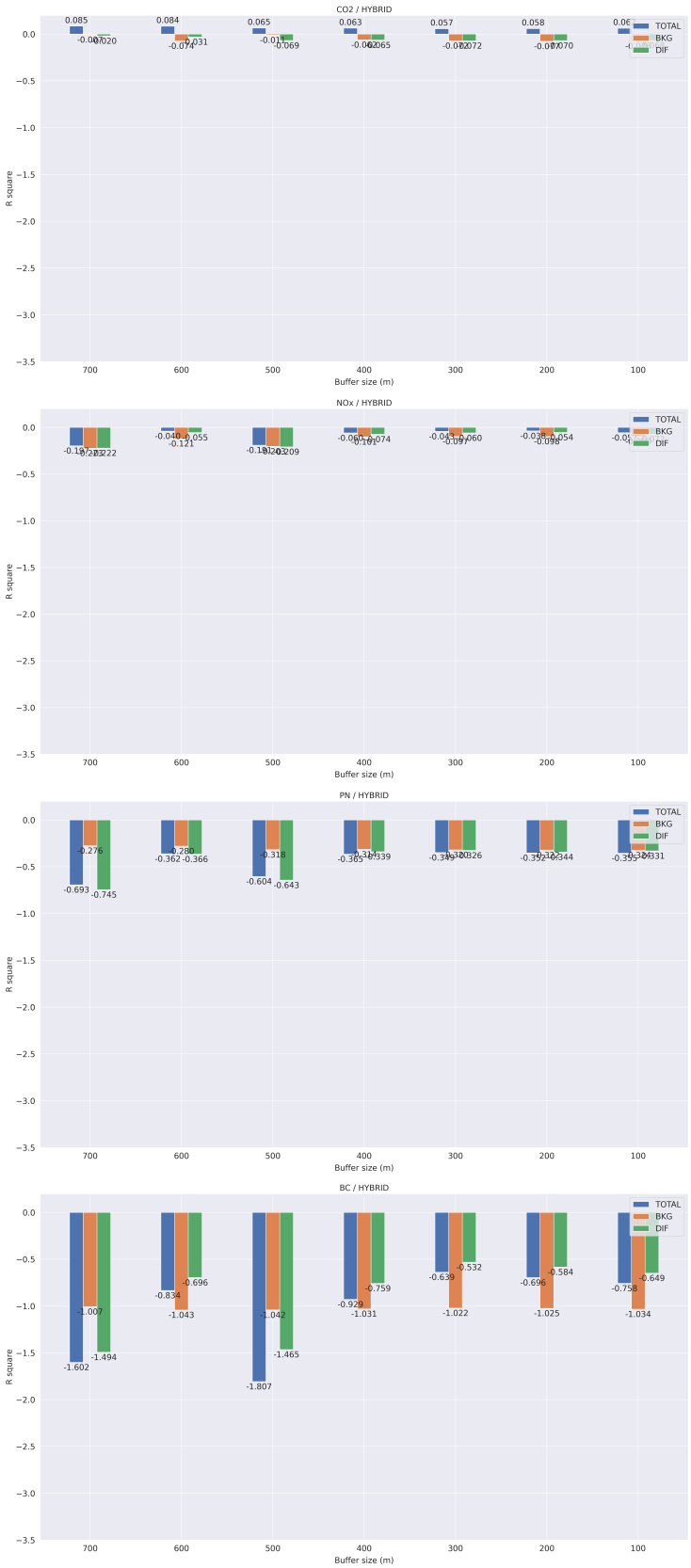

Figure A.7: HYBRID model sensitivity analysis of buffer size (Test-one-day with transfer learning)

doi:10.6342/NTU202202826

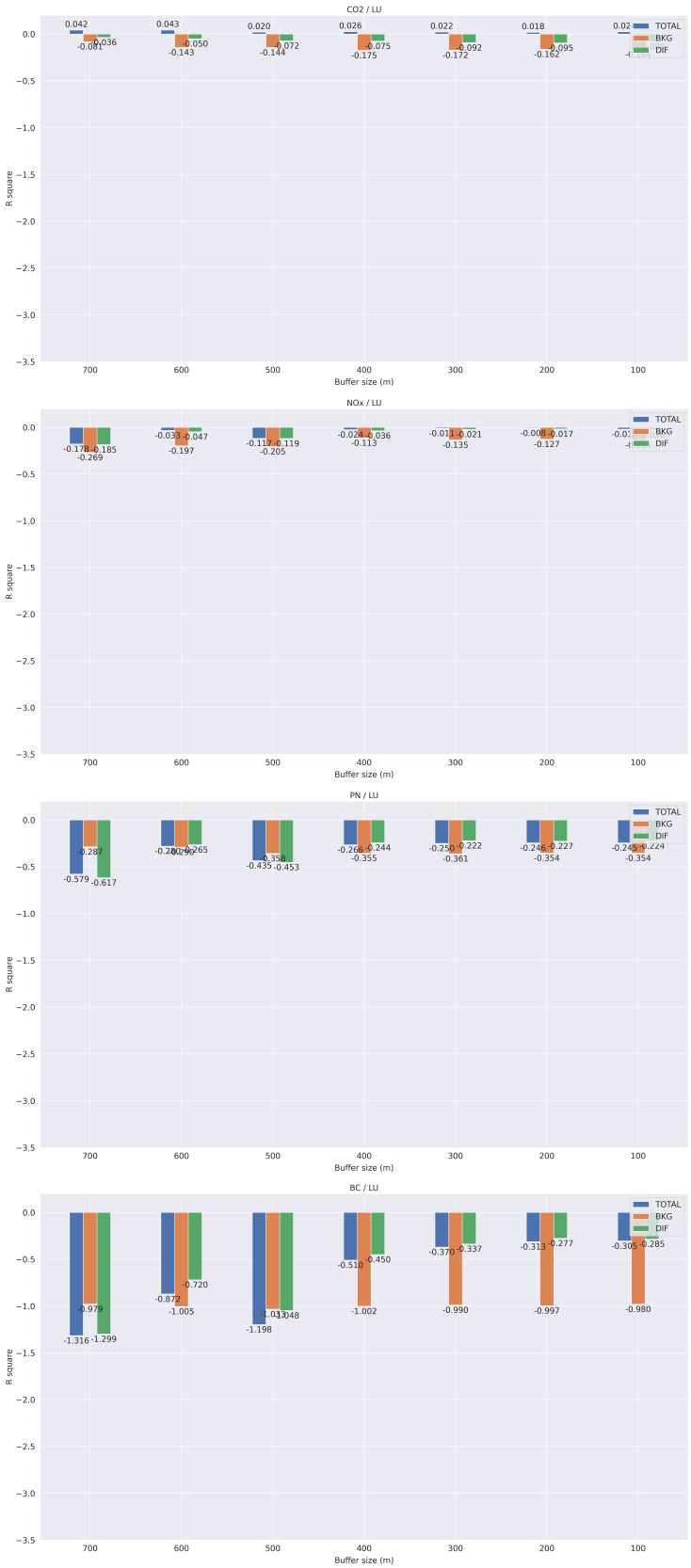

Figure A.8: LU model sensitivity analysis of buffer size (Test-one-day with transfer learning)

doi:10.6342/NTU202202826

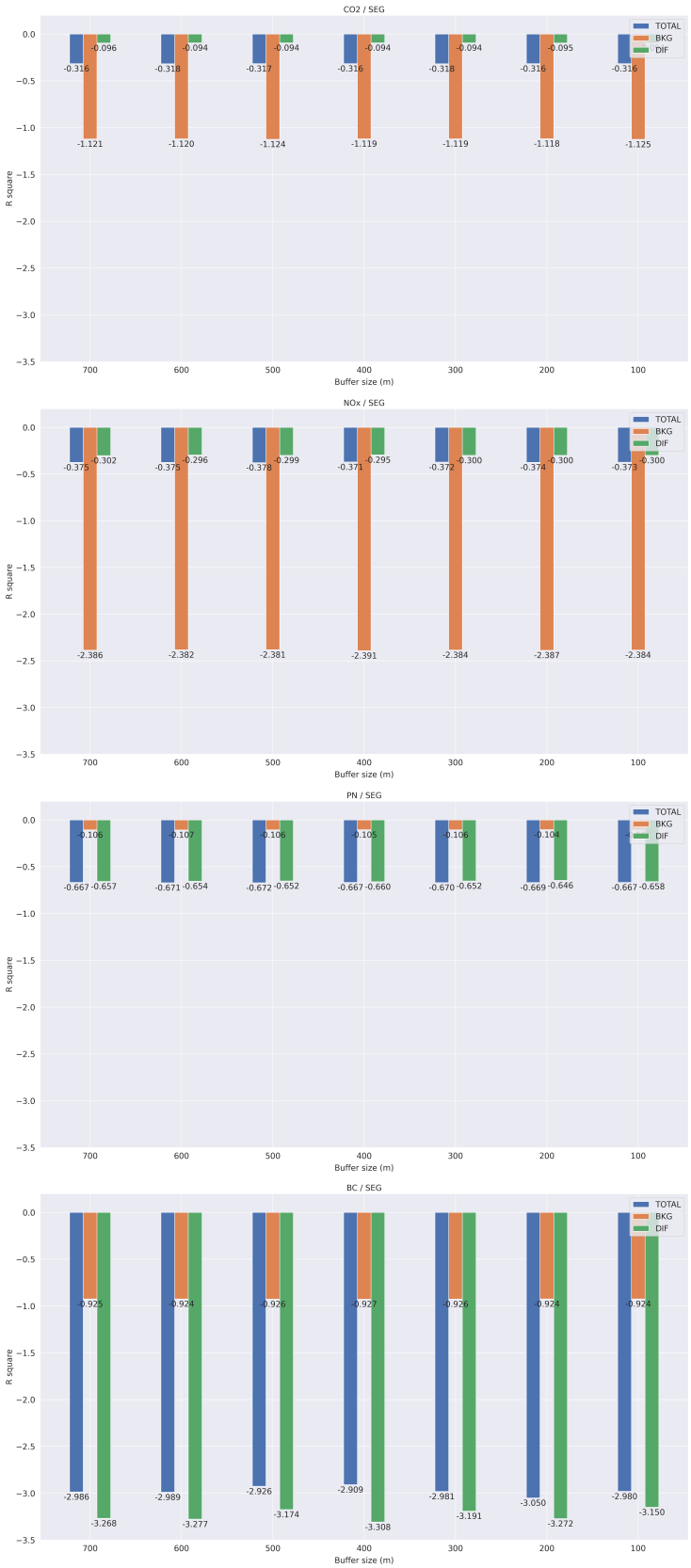

Figure A.9: SEG model sensitivity analysis of buffer size (Test-one-day with transfer learning)

doi:10.6342/NTU202202826

Appendix B — Land use

doi:10.6342/NTU202202826

類別代碼	類別名稱	R	G	B	色塊
01	農業利用土地	152	230	0	
0101	水田	209	255	115	
010101	水稻田	171	220	97	
010102	其他水田	110	221	97	
0102	旱田	233	255	190	
010201	旱作	198	230	150	
010202	茶園	56	204	61	
010203	雜作地	200	205	56	
0103	果園	126	237	39	
010301	香蕉果園	99	192	59	
010302	落葉果園	170	192	60	
010303	檳榔	142	169	68	
0104	水產養殖	138	255	218	
010400	水產養殖	138	255	218	
0105	畜牧	159	177	105	
010501	畜舍舍	112	134	79	
010502	牧場	147	203	62	
0106	農業相關設施	168	168	0	
010601	溫室	107	144	75	
010602	其他農業相關設施	77	101	57	

類別代碼	類別名稱	R	G	B	色塊
02	森林利用土地	90	194	0	
0201	針葉林	58	122	42	
020100	針葉林	58	122	42	
0202	闊葉林	56	168	0	
020200	闊葉林	56	168	0	
0203	竹林	79	190	15	
020300	竹林	79	190	15	
0204	混淆林	24	141	13	
020401	針闊葉混淆林	44	124	10	
020402	竹闊葉混淆林	74	162	37	
020403	竹針葉混淆林	36	97	10	
020404	竹針闊葉混淆林	35	81	16	
0205	灌木林	122	186	101	
020500	灌木林	122	186	101	
0206	其他森林利用土地	58	81	23	
020601	伐木跡地	193	169	71	
020602	苗圃	44	199	70	
020603	防火線	196	161	77	
020604	土壤	225	173	52	

類別代碼	類別名稱	R	G	B	色塊
03	交通利用土地	255	85	0	
0301	機場	174	120	255	
030100	機場	174	120	255	
030201	一般鐵路及相關設施	233	119	210	
030202	一般鐵路相關設施	176	87	158	
0303	高速鐵路及相關設施	109	0	189	
030301	高速鐵路	129	81	212	
030302	高速鐵路相關設施	99	62	162	
0304	捷運及相關設施	163	38	255	
030401	捷運路線	148	78	239	
030402	捷運相關設施	115	59	189	
0305	國道	230	0	0	
030500	國道	230	0	0	
0306	省道	255	120	120	
030600	省道	255	120	120	
0307	快速公路	255	20	165	
030700	快速公路	255	20	165	
0308	一般道路	231	148	163	
030800	一般道路	231	148	163	
0309	道路相關設施	211	142	191	
030901	停車場	143	120	174	
030902	其他道路相關設施	95	76	119	
0310	港口	103	141	174	
031001	商港	79	108	203	
031002	漁港	116	134	192	
031003	專用港	90	109	169	
031004	其他港口設施	63	72	101	

類別代碼	類別名稱	R	G	B	色塊
04	水利利用土地	151	219	242	
0401	河道	190	232	255	
040101	河川	164	215	245	
040102	溝渠	16	215	245	
040103	運河	110	199	250	
0402	堤防	156	156	156	
040200	堤防	156	156	156	
0403	濕地	166	205	213	
040300	濕地	166	205	213	
0404	水庫	70	212	206	
040400	水庫	70	212	206	
0405	湖泊	121	238	233	
040500	湖泊	121	238	233	
0406	蓄水池	158	215	194	
040600	蓄水池	158	215	194	
0407	水利設施	214	136	0	
040700	水利構造物	214	136	0	
0408	水閘門	53	95	96	
040801	水閘門	87	103	124	
040802	抽水站	112	143	161	
040803	水庫壩	90	133	158	
040804	地下取水井	36	120	168	
040805	其他水利設施	92	126	145	
0409	防汛道路	204	204	204	
040900	防汛道路	204	204	204	
0410	海面	158	202	255	
041000	海面	158	202	255	

類別代碼	類別名稱	R	G	B	色塊
05	建築利用土地	255	161	161	
0501	商業	194	0	6	
050101	零售批發	216	5	61	
050102	服務業	228	62	106	
0502	純住宅	255	244	41	
050200	純住宅	255	244	41	
0503	混合使用住宅	235	224	82	
050301	商工業使用住宅	202	178	26	
050302	農業使用住宅	228	180	25	
050303	其他使用住宅	236	193	83	
0504	製造業	255	194	61	
050400	製造業	255	194	61	
0505	倉儲	165	129	68	
050500	倉儲	165	129	68	
0506	宗教	197	0	255	
050600	宗教	197	0	255	
0507	殯葬設施	130	130	130	
050700	殯葬設施	130	130	130	
0508	其他建築用地	205	205	102	
050801	興建中	209	136	9	
050802	其他	186	104	73	

類別代碼	類別名稱	R	G	B	色塊
06	公共利用土地	255	197	89	
0601	政府機關	255	159	41	
060100	政府機關	255	159	41	
0602	學校	232	190	255	
060201	幼兒園	235	186	255	
060202	小學	227	158	255	
060203	中學	218	129	255	
060204	大專院校	209	101	235	
060205	特種學校	201	73	255	
0603	醫療保健	161	139	246	
060300	醫療保健	161	139	246	
0604	社會福利設施	249	224	165	
060400	社會福利設施	249	224	165	
0605	公用設備	255	218	150	
060501	警察	148	172	176	
060502	電力	147	161	232	
060503	瓦斯	239	114	135	
060504	自來水	164	175	232	
060505	加油站	123	153	148	
0606	殯葬設施	216	141	103	
060600	殯葬設施	216	141	103	

類別代碼	類別名稱	R	G	B	色塊
07	遊憩利用土地	255	251	20	
0701	文化設施	255	255	190	
070101	法定文化資產	205	205	93	
070102	一般文化設施	233	233	132	
070103	其他文化設施	230	230	147	
0702	公園綠地廣場	147	255	47	
070200	公園綠地廣場	147	255	47	
0703	休閒設施	191	255	191	
070301	遊樂場所	246	171	171	
070302	體育場所	172	172	247	

類別代碼	類別名稱	R	G	B	色塊
08	露營利用土地	206	140	255	
0801	露營及相關設施	206	153	29	
080100	露營及相關設施	206	153	29	
0802	土石及相關設施	149	111	35	
080200	土石及相關設施	149	111	35	
0803	礦業及相關設施	140	140	140	
080300	礦業及相關設施	140	140	140	

類別代碼	類別名稱	R	G	B	色塊
09	其他利用土地	225	225	225	
0901	溼地	0	168	132	
090100	溼地	0	168	132	
0902	裸生地	176	211	38	
090200	裸生地	176	211	38	
0903	裸露地	179	168	46	
090301	裸地	201	173	137	
090302	崩塌地	154	137	105	
090303	礫岩	192	108	34	
0904	暫未利用土地	51	51	51	
090400	暫未利用土地	51	51	51	
0905	空置地	255	236	201	
090501	未使用地	192	174	84	
090502	人工改變中土地	188	146	62	

Figure B.10: Land use classes

doi:10.6342/NTU202202826

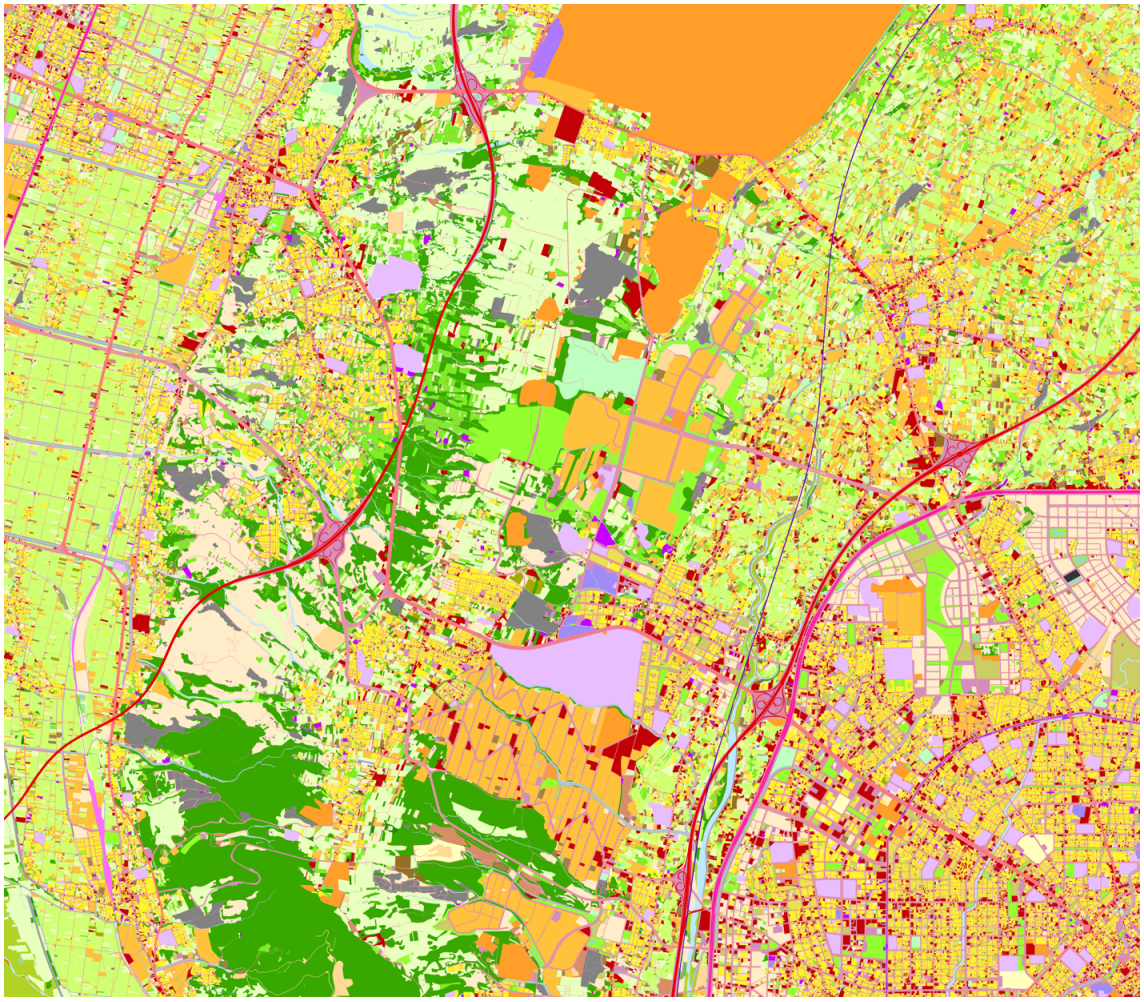

Figure B.11: Total land use distribution

doi:10.6342/NTU202202826